Copyright © 1977, by the author(s).
All rights reserved.

Permission to make digital or hard copies of all or part of this work for personal or classroom use is granted without fee provided that copies are not made or distributed for profit or commercial advantage and that copies bear this notice and the full citation on the first page. To copy otherwise, to republish, to post on servers or to redistribute to lists, requires prior specific permission.

THE HOPF BIFURCATION THEOREM AND ITS APPLICATIONS TO NONLINEAR OSCILLATIONS IN CIRCUITS AND SYSTEMS

by

A. I. Mees and L. O. Chua

Memorandum No. UCB/ERL M77/63

23 September 1977

ELECTRONICS RESEARCH LABORATORY

College of Engineering
University of California, Berkeley
94720

THE HOPF BIFURCATION THEOREM AND ITS APPLICATIONS TO NONLINEAR OSCILLATIONS IN CIRCUITS AND SYSTEMS[†]

A. I. Mees and L. O. Chua[††]

ABSTRACT

One of the most powerful methods for studying periodic solutions in autonomous nonlinear systems is the theory which has developed from a proof by E. Hopf. He showed that oscillations near an equilibrium point can be understood by looking at the eigenvalues of the linearized equations for perturbations from equilibrium, and at certain crucial derivatives of the equations. A good deal of work has been done recently on this theory and the present paper summarizes recent results, presents some new ones, and shows how they can be used to study almost sinusoidal oscillations in nonlinear circuits and systems. The new results are a proof of the basic part of the Hopf theorem using only elementary methods, and a graphical interpretation of the theorem for nonlinear lumped and distributed multiple-loop feedback systems. The graphical criterion checks the Hopf conditions for the existence of stable or unstable periodic oscillations. Since it is reminiscent of the generalized Nyquist criterion for linear systems, our graphical procedure can be interpreted as the frequency-domain version of the Hopf bifurcation theorem.

[†]This work is sponsored in part by the Office of Naval Research Contract N00014-76-0572 and by the Miller Institute which supported the second author during the 1976-77 Academic Year as a Miller Research Professor.

[††]A. I. Mees is with the Department of Pure Mathematics and Mathematical Statistics, University of Cambridge, Cambridge, England. L. O. Chua is with the Department of Electrical Engineering and Computer Sciences and the Electronics Research Laboratory, University of California, Berkeley, CA 94720.

1. INTRODUCTION

A standard procedure for designing an almost sinusoidal electronic oscillator is to bias a locally active device into its active region and then imbed it in an external frequency-dependent linear circuit [1]. The device could be any of a large variety of 2-terminal elements. For example, it could be characterized by a nonlinear dc V-I curve having a negative resistance region, as in the case of a tunnel diode [2], or by a nonlinear ac dynamic circuit model as in the case of a Gunn diode [3]. It could also be a 3-terminal device such as a transistor, or a multi-terminal device such as an operational amplifier [4]. The parameters of the external circuit are then chosen in such a way that the linearized circuit has a pair of complex-conjugate poles which lies slightly to the right of the $j\omega$-axis [1,4]. It is argued that thermal noise will generate an oscillation which grows until its amplitude is limited by the device's nonlinearity. In practice, the oscillation frequency is usually calculated to be the frequency ω_o at which the pole crosses the $j\omega$-axis, while the amplitude is often determined by a first-order harmonic balance (describing function) method [1]. While this approach usually works in practice, it is often inaccurate and appears to have no rigorous foundation. As a matter of fact, it is easy to find counterexamples where it fails.

One way to justify this common oscillator design procedure is to make the describing function analysis rigorous. This has been done for oscillator circuits containing a single nonlinearity in the feedback loop of a linear circuit which may contain both lumped and distributed elements [5,22,23,25,26]. The treatment which fits our present problem best was given by Kudrewicz and Odyniec [6] who investigated a bifurcation problem associated with a single-loop feedback system when a parameter μ is varied. They used a first-order harmonic balance approach and succeeded in deriving sufficient conditions for the existence of an oscillation when μ is close to a critical value μ_o. However, only one nonlinearity was allowed in their study and no stability analysis was given.

It appears that the best and most general approach for studying almost sinusoidal oscillations is the Hopf bifurcation theorem [7]. Interestingly enough, the basic assumption of this theorem is almost identical to that invoked by electronic engineers using the ad hoc method described earlier. In fact, the theory of the Hopf bifurcation has been widely applied in biology [8-9], physics [10-11], and chemistry [12]. The purpose of this paper is to show how it can be equally useful in circuits and systems. The type of problem where it is useful is one in which an autonomous nonlinear system has an equilibrium state and there

is a parameter μ (either naturally occurring or artificially introduced) whose variation causes the equilibrium state to change its local stability properties. The question is, under what circumstances will the appearance of a periodic solution be associated with the change in stability of the equilibrium? Having answered this, one can then ask associated questions concerning uniqueness, stability and persistence of the periodic solution.

Loosely, the theorem says that if on linearizing the equation about an equilibrium point we find that pairs of complex conjugate eigenvalues cross the imaginary axis as μ varies through certain critical values, then for near-critical values of μ there are limit cycles close to the equilibrium point. Just how near to criticality μ has to be is not determined, and indeed unless a certain rather complicated expression is non-zero, existence is only assured exactly at criticality. The sign of the expression determines the stability of the limit cycle, and whether the limit cycle exists for subcritical ($\mu<\mu_o$) or supercritical ($\mu>\mu_o$) parameter values. (We are adopting the convention that near $\mu = \mu_o$ the real parts of the relevant eigenvalues increase as μ increases.) One way to prove this theorem is to use the geometrical approach of Ruelle and Takens [11], described at length by Marsden and McCracken [10]. This gives a very clear picture of what is going on and we shall describe it first, in Sec. 2, with a new proof of the basic existence result. Poore [13] proves the theorem by methods which are related to those of [10], but which involve less algebra, but we shall not describe his proof here.

An alternative approach is to try a series solution of the differential equations. This was what Hopf did originally [7] and a recent writer adopting the same general attitude is Allwright [14], though his method differs in important respects from Hopf's. In Sec. 3, we shall review this contribution because it gives the result in a form that is adapted to circuit and system theoretic problems, and because it is based on harmonic balancing, a technique well known in systems theory. Allwright's approach is, in some respects, similar to that of Kudrewicz and Odyniec [6], although it was developed independently. However, his method allows multiple nonlinearities and is more accurate because he uses a second-order harmonic balance method. Moreover, he gave a graphical interpretation for detecting the existence of a periodic oscillation in single-loop feedback systems. He also made a rigorous stability analysis. The end result of Allwright's approach is precisely the Hopf bifurcation theorem, but his proof is substantially shorter than other proofs known to the present authors. In view of its practical significance, our main objective in the later part of this paper is to generalize Allwright's graphical method to multiple-loop feedback systems.

Another objective of this paper is to present a unified treatment of the Hopf bifurcation theorem from two different perspectives, and then show how this theorem can be used to explain oscillatory phenomena arising from nonlinear circuits and systems. In so doing, we will try to filter out the relevant aspects of this theorem which are too often buried under a morass of unwieldy algebra and abstractions. However, since there is now an extensive literature on the theory [10,11,13,14], we shall not prove all results completely. Whenever applicable, we shall indicate methods of proof while referring to the sources that seem to give the clearest exposition. We shall, however, give a new and hopefully more enlightening proof of the basic part of the theorem.

To distinguish between the two equivalent approaches for deriving the Hopf bifurcation theorem, we shall refer to the first as a "time-domain approach" because all analysis is based on the differential equations. In contrast to this, the second approach is based on feedback systems and is similar to the generalized Nyquist stability criterion for linear systems [15]: it will therefore be referred to as a "frequency-domaim approach." Since the statements of the theorem are different in the two approaches, they will be called respectively the "time-domain" and the "frequency-domain" Hopf bifurcation theorem.

Finally, in Sec. 4, we give some examples to illustrate the theorem. It has sometimes been used without a complete appreciation of its advantages and disadvantages, so we emphasize the geometrical ideas of Sec. 2 as an aid to intuition in applications. In particular, we explain the importance of the local nature of the theorem: in its usual form it only makes predictions for unspecified -- possibly very small — regions of parameter space and state space. As long as this is borne in mind a lot of useful information can be obtained, though obviously it is desirable to be able to estimate the size of the regions. (This latter problem, the principal weakness of the Hopf bifurcation theorem, is partially alleviated by the new approach of Sec. 2 and by a recent result due to Swinnerton Dyer [16].)

2. The Hopf Bifurcation in the Time Domain

2.1. The two-dimensional case

The geometrical idea behind the Hopf bifurcation is best seen by observing how the phase portrait of a parameterized two-dimensional system

$$\dot{x}_1 = f_1(x_1, x_2; \mu) \tag{1a}$$

$$\dot{x}_2 = f_2(x_1, x_2; \mu) \tag{1b}$$

might alter as the parameter μ is varied. To be specific, let $\hat{\underset{\sim}{x}} = [\hat{x}_1, \hat{x}_2]^T$ be an equilibrium point of (1), where $\hat{\underset{\sim}{x}}$ may depend on μ. Now suppose this equilibrium point changes from a spiral sink (a stable focus) to a spiral source (an unstable focus) as μ increases from $\mu_o - \varepsilon$ to $\mu_o + \varepsilon$. Now suppose that at the critical value $\mu = \mu_o$, the equilibrium point is a center, i.e., the local linearization gives rise to undamped simple harmonic motion of period $2\pi/\omega_o$, where $\pm i\omega_o$ are the eigenvalues of the Jacobian matrix evaluated at $\underset{\sim}{x} = \hat{\underset{\sim}{x}}$ at criticality ($\mu = \mu_o$). Very close to the equilibrium point, the system behaves as if it is linear. But a little further out, the effects of nonlinearity sometimes manifest themselves in the appearance of a limit cycle. Figures 1(a) and (b) show two qualitatively distinct phase portraits associated with two systems having an identical equilibrium point and Jacobian matrix. Observe that while the phase portraits in Figs. 1(a) and 1(b) are identical in a small neighborhood of the equilibrium point, they differ drastically farther out. In particular, the limit cycle in Fig. 1(a) is stable and occurs only after criticality (supercritical case) whereas that in Fig. 1(b) is unstable and occurs only before criticality (subcritical case).

A somewhat better picture of what is happening can be seen in the (x_1, x_2, μ) space as shown in Figs. 2(a) and (b), respectively. Here, the slices with constant μ are phase portraits and we have represented loci of attractors (or more precisely, loci of minimal attractors) by heavy solid lines, and loci of repellors by heavy dashed lines. Thus the "bowl" in each case represents the loci of limit cycles parameterized by μ. In Fig. 2(a), corresponding to Fig. 1(a), an attracting limit cycle appears as μ reaches criticality and grows as μ increases further, while in Fig. 2(b), corresponding to Fig. 1(b), an unstable limit cycle gets smaller as μ increases, disappearing as μ reaches criticality. In both cases, the equilibrium point is locally attracting for $\mu < \mu_o$ and repelling for $\mu > \mu_o$.

We can distinguish between the two cases by observing whether the bowl is the right way up, as in Fig. 2(a), or upside down, as in Fig. 2(b). It turns out that this criterion can be generalized for n-dimensional systems (n>2), and in fact the complicated expression mentioned earlier is just a negative constant times the curvature of the bowl at $\mu = \mu_o$. It is interesting to observe that if the curvature is

non-vanishing, the bowl is parabolic so that the maximum amplitude of the limit cycle grows as $|\mu-\mu_o|^{1/2}$; i.e., much faster than $|\mu-\mu_o|$ intitially. Hence, even though the amplitude is zero at criticality,[1] it grows rapidly into a respectable magnitude just slightly beyond or before criticality. This phenomenon is consistent with that normally observed in almost all nearly sinusoidal electronic oscillators [1]. If the curvature vanishes, it is possible, though not certain, that the bowl is flat out to infinity, in which case the limit cycle exists only at the critical value $\mu = \mu_o$ and hence has zero amplitude. An example of this degenerate case is given by $\dot{x}_1 = x_2$, $\dot{x}_2 = -\mu x_2 - x_1$, where criticality occurs at $\mu = 0$. An example where the curvature vanishes yet the bowl is not flat is given by $\dot{x}_1 = x_2$, $\dot{x}_2 = -\mu x_2 - x_1 + g(x_1,x_2)$, where all partial derivatives of $g(\cdot)$ at the origin vanish up to 4th order, but there is a nonvanishing 5th partial derivative.

To prove the theorem, Marsden and McCracken [10] use the implicit function theorem to guarantee that the bowl exists sufficiently close to criticality. They also show how to calculate the curvature so as to ensure that the predicted limit cycles are not degenerate ones, and to determine whether they are attracting or repelling. Unfortunately the implicit function theorem proof leads to extremely heavy algebra, particularly in the derivation of the curvature, which occupies many pages in Marsden and McCracken's book and is claimed to take a month to check properly. If we are prepared to prove only existence but not uniqueness (and so to lose a proper stability proof) we can proceed much more directly by using Lyapunov's second method. The key idea is the realization that the difference between case (a) and case (b) of Fig. 2 is whether the equilibrium is attracting or repelling <u>at criticality</u>: when $\mu = \mu_o$ the equilibrium $\hat{\underset{\sim}{x}}$ is attracting if and only if the bowl is the right way up and repelling if and only if it is upside down. Of course, the attraction or repulsion must be due entirely to nonlinear effects since the eigenvalues of the linearized equations have zero real parts when $\mu = \mu_o$. The terms <u>vague attractor</u> and <u>vague repeller</u> are used to describe the equilibrium at criticality.

Our goal in this section is to present a simple proof of the "existence" part of the Hopf theorem in a neighborhood of an equilibrium point

---

[1] The limit cycle of the nonlinear system at criticality should not be confused with the continuum of periodic orbits of the associated linearized system at criticality. While the former has zero amplitude, the latter can have any amplitude. Notice that we are following the traditional usage where a periodic orbit is called a limit cycle only if it is isolated.

$\hat{\underset{\sim}{x}}(\mu) = \left(\hat{x}_1(\mu), \hat{x}_2(\mu)\right)$ of (1). We assume that the function $\underset{\sim}{f}(\underset{\sim}{x};\mu)$ is C^k $(k \geq 4)$ jointly in $\underset{\sim}{x}$ and μ. We assume further that at $\mu = \mu_o$, the associated Jacobian matrix has a pair of simple complex-conjugate eigenvalues $\lambda(\mu)$ and $\bar{\lambda}(\mu)$, where $\lambda(\mu) = \alpha(\mu) + i\omega(\mu)$, $\alpha(\mu_o) = 0, \alpha'(\mu_o) > 0$, and $\omega(\mu_o) \neq 0$. We next follow Marsden and McCracken by transforming coordinates so that (1) becomes

$$\dot{x}_1 = \tilde{f}_1(x_1, x_2; \mu) \tag{2a}$$

$$\dot{x}_2 = \tilde{f}_2(x_1, x_2; \mu) \tag{2b}$$

where the origin (0,0) becomes the new equilibrium point (independent of μ) and the associated Jacobian matrix assumes the standard form

$$(D\underset{\sim}{\tilde{f}})(0;\mu) = \begin{bmatrix} \alpha(\mu) & \omega(\mu) \\ -\omega(\mu) & \alpha(\mu) \end{bmatrix} \tag{2c}$$

where $\omega \neq 0$ for all μ, while $\alpha(\mu) < 0$ if $\mu < \mu_o$ and $\alpha(\mu) > 0$ if $\mu > \mu_o$.

We want to construct a Lyapunov function V to test stability of the origin. Because we have to take account of higher order derivatives than the first, a quadratic V will not do: to ensure sign definiteness of $\dot{V}$ (at least when x is close enough to x=0), we need quartic terms. Thus we choose:

$$\begin{aligned} V = {} & \frac{1}{2}(x_1^2 + x_2^2) \\ & + \frac{1}{3}ax_1^3 + bx_1^2x_2 + cx_1x_2^2 + \frac{1}{3}dx_2^3 \\ & + \frac{1}{4}ex_1^4 + gx_1^3x_2 + \frac{1}{2}hx_1^2x_2^2 + jx_1x_2^3 + \frac{1}{4}kx_2^4 \end{aligned} \tag{3}$$

and try to pick the constants a, b, ..., k to give $\dot{V}$ the properties we want. This task is not as fearsome as it seems, since it can be done in stages. Let us first expand $\underset{\sim}{\tilde{f}}(\underset{\sim}{x};\mu)$ about the origin via Taylor's theorem and make use of (2c) to obtain

$$\dot{x}_1 = \alpha(\mu)x_1 + \omega(\mu)x_2 + O(|\underset{\sim}{x}|^2) \tag{4a}$$

$$\dot{x}_2 = -\omega(\mu)x_1 + \alpha(\mu)x_2 + O(|\underset{\sim}{x}|^2) \tag{4b}$$

where $O(|\underset{\sim}{x}|^2)$ denotes the terms of order higher than the first.[2] Next, we calculate the time derivative of V along the trajectories of (4) in a neighborhood of the origin; namely,

$$\dot{V} = \alpha(\mu)\ (x_1^2+x_2^2) + O(|\underset{\sim}{x}|^4) \tag{5}$$

It follows from (5) that for small $|\underset{\sim}{x}|$, $\dot{V}$ is negative definite when $\alpha(\mu) < 0$ but positive definite when $\alpha(\mu) > 0$, <u>independent</u> of the coefficients a, b, ..., k in (3). Hence, it only remains to examine the case $\alpha(\mu) = 0$. Since we will have to look at higher order terms in this case, let us expand (4) to include 2nd and 3rd order terms:

$$\dot{x}_1 = \alpha\ (\mu)x_1 + \omega(\mu)x_2 + \frac{1}{2}\tilde{f}^1_{11}x_1^2 + \tilde{f}^1_{12}x_1x_2 + \frac{1}{2}\tilde{f}^1_{22}x_2^2 + \frac{1}{6}\tilde{f}^1_{111}x_1^3 + \frac{1}{2}\tilde{f}^1_{112}x_1^2x_2$$

$$+ \frac{1}{2}\tilde{f}^1_{122}x_1x_2^2 + \frac{1}{6}\tilde{f}^1_{222}x_2^3 + O(|\underset{\sim}{x}|^4) \tag{6a}$$

$$\dot{x}_2 = -\omega(\mu)x_1 + \alpha(\mu)x_2 + \frac{1}{2}\tilde{f}^2_{11}x_1^2 + \tilde{f}^2_{12}x_1x_2 + \frac{1}{2}\tilde{f}^2_{22}x_2^2 + \frac{1}{6}\tilde{f}^2_{111}x_1^3 + \frac{1}{2}\tilde{f}^2_{112}x_1^2x_2$$

$$+ \frac{1}{2}\tilde{f}^2_{122}x_1x_2^2 + \frac{1}{6}\tilde{f}^2_{222}x_2^3 + O(|\underset{\sim}{x}|^4) \tag{6b}$$

where

$$\tilde{f}^i_{pq} \triangleq \left.\frac{\partial^2 \tilde{f}_i}{\partial x_p \partial x_q}\right|_{\underset{\sim}{x}=\underset{\sim}{0}} \quad \text{and} \quad \tilde{f}^i_{pqr} \triangleq \left.\frac{\partial^3 \tilde{f}_i}{\partial x_p \partial x_q \partial x_r}\right|_{\underset{\sim}{x}=\underset{\sim}{0}}$$

are generally functions of μ. The corresponding expression for $\dot{V}$ is now given by:

---

[2] If $\underset{\sim}{x} \in \mathbb{R}^n$ we write $|\underset{\sim}{x}|$ for $\sqrt{\sum_{i=1}^{n} |x_i|^2}$. To simplify writing out unwieldy but often irrelevant expressions, we will frequently use the well-known "Big O" notation [17]; namely, we will write $\underset{\sim}{p}(\underset{\sim}{x}) = O(\underset{\sim}{q}(\underset{\sim}{x}))$ in a neighborhood of $\underset{\sim}{x}_o$ if there exists a constant A such that $|\underset{\sim}{p}(\underset{\sim}{x})| \leq A|\underset{\sim}{q}(\underset{\sim}{x})|$ as $\underset{\sim}{x} \to \underset{\sim}{x}_o$. For example, we will write $\sum_{\ell=m}^{\infty}\sum_{k=0}^{\ell} a_{k\ell}x_1^k x_2^{\ell-k}$ as $O(|\underset{\sim}{x}|^m)$ in a neighborhood of $\underset{\sim}{x} = \underset{\sim}{0}$. Similarly, we will write $\underset{\sim}{p}(\underset{\sim}{x}) = O(1)$ if $\underset{\sim}{p}(\underset{\sim}{x})$ is bounded in a neighborhood of $\underset{\sim}{0}$.

$$\dot{V} = \alpha\left(x_1^2+x_2^2\right) + \left(-\omega b + \frac{1}{2}\tilde{f}^1_{11}\right)x_1^3 + \left(\omega c + \frac{1}{2}\tilde{f}^2_{22}\right)x_2^3 + \left(\omega(a-2c) + \tilde{f}^1_{12} + \frac{1}{2}\tilde{f}^2_{11}\right)x_1^2x_2$$
$$+ \left(\omega(2b-d) + \frac{1}{2}\tilde{f}^1_{22} + \tilde{f}^2_{12}\right)x_1x_2^2 + \left(-\omega g + \frac{1}{2}a\,\tilde{f}^1_{11} + \frac{1}{2}b\tilde{f}^2_{11} + \frac{1}{6}\tilde{f}^1_{111}\right)x_1^4$$
$$+ \left(\omega(e-h) + b\tilde{f}^1_{11} + a\tilde{f}^1_{12} + c\tilde{f}^2_{11} + b\tilde{f}^2_{12} + \frac{1}{2}\tilde{f}^1_{112} + \frac{1}{6}\tilde{f}^2_{111}\right)x_1^3x_2$$
$$+ \left(3\omega(g-j) + \frac{1}{2}c\tilde{f}^1_{11} + 2b\tilde{f}^1_{12} + \frac{1}{2}a\tilde{f}^1_{22} + \frac{1}{2}d\tilde{f}^2_{11} + 2c\tilde{f}^2_{12} + \frac{1}{2}b\tilde{f}^2_{22} + \frac{1}{2}\tilde{f}^1_{122} + \frac{1}{2}\tilde{f}^2_{112}\right)x_1^2x_2^2$$
$$+ \left(\omega(h-k) + c\tilde{f}^1_{12} + b\tilde{f}^1_{22} + d\tilde{f}^2_{12} + c\tilde{f}^2_{22} + \frac{1}{6}\tilde{f}^1_{222} + \frac{1}{2}\tilde{f}^2_{122}\right)x_1x_2^3$$
$$+ \left(\omega j + \frac{1}{2}c\tilde{f}^1_{22} + \frac{1}{2}d\tilde{f}^2_{22} + \frac{1}{6}\tilde{f}^2_{222}\right)x_2^4 + O(\alpha)\cdot O(|\underset{\sim}{x}|^4) + O(|\underset{\sim}{x}|^5) \qquad (7)$$

where we simply write α and ω for $\alpha(\mu)$ and $\omega(\mu)$. Since cubic terms prevent sign definiteness, we must make them all vanish by equating the coefficients of x_1^3, x_2^3, $x_1^2x_2$ and $x_1x_2^2$ in (7) to zero. This determines the coefficients a, b, c, and d uniquely as listed in Table 1. Likewise, we must force the fourth-order terms $x_1^3x_2$ and $x_1x_2^3$ to vanish by equating the respective coefficients in (7) to zero. This determines e and k as listed in Table 1.

Recall that we already know $\dot{V}$ is sign definite when $\alpha(\mu) \neq 0$. Now for $\dot{V}$ to be negative (resp., positive) definitive when $\alpha(\mu) = 0$, we need x_1^4 and x_2^4 to have negative (resp., positive) coefficients β_1 and β_3 in (7) and $x_1^2x_2^2$ to have a non-positive (resp., non-negative) coefficient β_2; namely,

Conditions for $\dot{V} < 0$	Conditions for $\dot{V} > 0$
$\beta_1 - \omega(\mu)g < 0$	$\beta_1 - \omega(\mu)g > 0$
$\beta_2 + 3\omega(\mu)(g-j) \leq 0$	$\beta_2 + 3\omega(\mu)(g-j) \geq 0$ (8)
$\beta_3 + \omega(\mu)j < 0$	$\beta_3 + \omega(\mu)j > 0$

where

$$\left.\begin{aligned}
\beta_1 &\triangleq \frac{1}{2}a\hat{f}^1_{11} + \frac{1}{2}b\hat{f}^2_{11} + \frac{1}{6}\hat{f}^1_{111} \\
\beta_2 &= \frac{1}{2}c\hat{f}^1_{11} + 2b\hat{f}^1_{12} + \frac{1}{2}a\hat{f}^1_{22} + \frac{1}{2}d\hat{f}^2_{11} + 2c\hat{f}^2_{12} + \frac{1}{2}b\hat{f}^2_{22} + \frac{1}{2}\hat{f}^1_{122} + \frac{1}{2}\hat{f}^2_{112} \\
\beta_3 &= \frac{1}{2}c\hat{f}^1_{22} + \frac{1}{2}d\hat{f}^2_{22} + \frac{1}{6}\hat{f}^2_{222}.
\end{aligned}\right\} \qquad (9)$$

These three inequalities are necessary conditions which must be satisfied by

both g and j simultaneously. Only the first and third inequalities are listed in Table 1 opposite g and j, respectively to save space. Observe that unlike the constraints on the coefficients a, b, c, and d which are fixed once the function $\tilde{f}(\underset{\sim}{x},\mu)$ is given, the inequality constraints given by (8) provide us with some "slack" to derive a simpler yet equivalent constraint. In particular, we can try to choose g and j such that the non-zero quartic terms in (7) are a perfect square

$$\sigma(x_1^2+x_2^2)^2 = \sigma x_1^4 + 2\sigma x_1^2 x_2^2 + \sigma x_2^4 . \tag{10}$$

Here σ is a parameter yet to be determined.[3] Equating the coefficients of the corresponding terms in (7) and (10), we obtain

$$\begin{aligned} \beta_1 - \omega(\mu)g &= \sigma \\ \beta_2 + 3\omega(\mu)(g-j) &= 2\sigma \\ \beta_3 + \omega(\mu)j &= \sigma \end{aligned} \tag{11}$$

where β_1, β_2, and β_3 are defined earlier in (9). Observe that while β_1, β_2, and β_3 are independent of g and j, they are functions of μ since the parameters a, b, c, and d in Table 1 depend on μ. Solving for σ from (11), we obtain

$$8\sigma(\mu) = 3(\beta_1+\beta_3) + \beta_2 \tag{12}$$

where $\sigma = \sigma(\mu)$ is a C^2 function of μ. Substituting the coefficients a, b, c, d, e, h, and k as defined in Table 1 into (7) and making use of (12), we obtain

$$\boxed{\dot{V} = \alpha(x_1^2+x_2^2) + \sigma(x_1^2+x_2^2)^2 + \alpha\, O(|\underset{\sim}{x}|^4) + O(|\underset{\sim}{x}|^5)} \tag{13}$$

Now at criticality ($\mu=\mu_o$), we have $\alpha(\mu_o) = 0$, and $\omega_o \triangleq \omega(\mu_o) \neq 0$. Hence, (writing σ_o for $\sigma(\mu_o)$), (13) implies that $\sigma_o < 0$ (resp., $\sigma_o > 0$) is sufficient to guarantee $\dot{V} < 0$ (resp., $\dot{V} > 0$) at criticality. That this condition is also necessary follows immediately from (8). Hence, we have proved that the

[3] Since the coefficients of the 3 non-zero quartic terms x_1^4, $x_1^2x_2^2$, and x_2^4 involve only 2 parameters g and j, we need to introduce a new parameter σ in order for the quartic terms to form a perfect square.

necessary and sufficient condition for $\dot{V}$ to be negative definite (resp., positive definite) at criticality is given by $\sigma_o < 0$ (resp., $\sigma_o > 0$). It is indeed remarkable that the sign of the single parameter σ_o -- henceforth called the curvature coefficient — completely determines the sign of $\dot{V}$ at criticality. Substituting the definitions of a, b, c, and d (with $\mu = \mu_o$) from Table 1 into (9) and (12), we obtain the following explicit expression:

$$4\sigma_o = \frac{1}{\omega_o}\left\{\tilde{f}^1_{11}(\tilde{f}^2_{11}-\tilde{f}^1_{12}) + \tilde{f}^2_{22}(\tilde{f}^2_{12}-\tilde{f}^1_{22}) + (\tilde{f}^2_{11}\tilde{f}^2_{12}-\tilde{f}^1_{12}\tilde{f}^1_{22})\right\} + (\tilde{f}^1_{111}+\tilde{f}^1_{122}+\tilde{f}^2_{112}+\tilde{f}^2_{222}) \tag{14}$$

where $\omega_o \triangleq \omega(\mu_o)$ and $\hat{f}^i_{jk}$ and $\hat{f}^i_{jk\ell}$ are all evaluated at $\underset{\sim}{x} = \underset{\sim}{0}$ and $\mu = \mu_o$. Let us now summarize the above results into the form of a lemma.

Lemma 1.

At criticality ($\mu=\mu_o$), the equilibrium point $\hat{\underset{\sim}{x}}(\mu_o)$ of (1), is a vague attractor if $\sigma_o < 0$ and a vague repeller if $\sigma_o > 0$, where σ_o is the curvature coefficient defined in (14).

It is reassuring to observe that our curvature coefficient in (14) is identical -- apart from an irrelevant factor $3\pi/\omega_o$ — to that derived by Marsden and McCracken (see their expression for $V'''(0)$ on p. 133) via a much more involved method.[4] The factors of 4 and 8 in (14) and (12) are also irrelevant but are included here in order for σ_o to be consistent with a more general definition we shall make in Sec. 3.

Observe that when $\sigma_o = 0$, we can say nothing at all. To investigate this case, we would have to generate a higher order Lyapunov Function — a tedious but not an intrinsically difficult task. We can now make use of the above results to prove a partial version of the Hopf Bifurcation theorem in $\mathbb{R}^2$ which merely asserts the existence of a limit cycle and which only provides a partial stability property.

Theorem 1. Partial version of Hopf bifurcation theorem in $\mathbb{R}^2$

Suppose the curvature coefficient associated with the equilibrium point

[4] Marsden and McCracken assumed $\omega(\mu) > 0$ which is why the factor $1/\omega_o$ is irrelevant. Our expression allows $\omega_o < 0$ which gives a small extra degree of flexibility in use.

$\hat{\underset{\sim}{x}}(\mu_o)$ of (1) does not vanish, i.e., $\sigma_o \neq 0$. Then there is an open neighborhood $\mathcal{N}$ of μ_o and for each $\mu \in \mathcal{N}$, $\hat{\underset{\sim}{x}}(\mu)$ has open neighborhoods $\mathcal{O}$ and $\mathcal{P}$ of diameter ε and ε' respectively, where $\varepsilon = O(|\alpha|^{1/2})$ and $\varepsilon' = O(1)$. For each $\mu \in \mathcal{N}$, writing $\alpha = \alpha(\mu)$ and $\hat{\underset{\sim}{x}} = \hat{\underset{\sim}{x}}(\mu)$, the following statements are true:

(a) If $\alpha\sigma_o \geq 0$ and $\sigma_o < 0$ (resp., $\sigma_o > 0$), $\hat{\underset{\sim}{x}}$ attracts (resp., repels) all points lying in $\mathcal{P}$.

(b) If $\alpha\sigma_o < 0$ there is at least one limit cycle lying within the closure of $\mathcal{O}$. If $\sigma_o < 0$ (resp., $\sigma_o > 0$), one such limit cycle attracts (resp., repels) all points inside it except $\hat{\underset{\sim}{x}}$, and one such (not necessarily distinct) limit cycle attracts (resp., repels) all points outside it and contained in $\mathcal{P}$.

Proof. Since the coordinate transformation from (1) to (2) is analytic and has an analytic inverse, we need only prove the theorem for (2). Now V in (3) is positive definite in an open neighborhood of the origin of size O(1). Call this $\tilde{\mathcal{P}}$, and let $\mathcal{P}$ be the corresponding neighborhood of $\hat{\underset{\sim}{x}}(\mu)$ in (1). The contours of V, i.e., the level curves $V^{-1}(\gamma)$, are approximately circular in $\tilde{\mathcal{P}}$ and, if $\tilde{\mathcal{P}}$ has been chosen small enough, they are nested in the sense that every steepest descent curve starting on the boundary of $\tilde{\mathcal{P}}$ leads to the origin (i.e., V has only one local minimum in $\tilde{\mathcal{P}}$, viz. $\underset{\sim}{0}$).

Notice that $\sigma(\mu) = \sigma_o + O(\mu-\mu_0)$ so if $\mathcal{N}$ has been chosen small enough, $\sigma(\mu)$ and σ_o have the same sign. Thus we can work with $\sigma = \sigma(\mu)$ throughout. For definiteness, take $\sigma < 0$; the case $\sigma > 0$ is exactly analogous. Then writing α for $\alpha(\mu)$, $\dot{V}$ is negative definite on $\tilde{\mathcal{P}}$ when $\alpha < 0$. Hence, the origin attracts $\tilde{\mathcal{P}}$ when $\alpha < 0$.

When $\alpha > 0$ (so $\alpha\sigma<0$) the sign definiteness properties of $\dot{V}$ for small $|\underset{\sim}{x}|$ and large $|\underset{\sim}{x}|$ are opposite to each other. We shall show that there is an annulus $\mathcal{R}$, bounded by two V contours, such that all trajectories in $\mathcal{N}$ but outside of $\mathcal{R}$ must eventually enter $\mathcal{R}$. Writing $r^2 = x_1^2 + x_2^2$, we see that $V = \gamma$ when

$$r^2 = 2\gamma + O(\gamma^{3/2})$$

which implies

$$\dot{V} = 2\gamma(\alpha+2\sigma\gamma) + \alpha O(\gamma^{3/2}) + O(\gamma^{5/2})$$

Thus if $r > 0$, $\dot{V}$ vanishes when $\gamma = -\alpha/2\sigma + O(\alpha^{3/2})$. There are therefore two values γ_1 and γ_2 of γ, both within $O(\alpha^{3/2})$ of $\gamma_o = -\alpha/2\sigma$, for which $\gamma < \gamma_1$ implies $\dot{V} > 0$ and $\gamma > \gamma_2$ implies $\dot{V} < 0$. Thus all trajectories in $\mathcal{N}$ must enter

the annulus[5]

$$\mathcal{R} = \{V^{-1}(\gamma) \mid \gamma_1 \leq \gamma \leq \gamma_2\}.$$

We now have an annulus which is positively invariant and contains no equilibria. It follows from the Poincare-Bendixon theorem [18] that the annulus contains at least one limit cycle and therefore the closure of $\mathcal{O} = \{\underset{\sim}{x} \mid V(\underset{\sim}{x}) < \gamma_2\}$ contains at least one limit cycle. The stability properties follow at once. ¤

Remarks.

1. Note that γ_o corresponds to $r^2 = -\alpha/\sigma$, so in the transformed coordinates each of the limit cycles are nearly a circle centered at the origin and of radius $|\alpha/\sigma|^{1/2}$; in fact they all lie within $O(\alpha^{3/2})$ of this circle.

2. Theorem 1 differs from the usual statement of the Hopf theorem in that it fails to guarantee that the limit cycle is unique and it does not provide an estimate for the period of oscillation (though this could be done fairly easily). In fact, if $\alpha'(\mu_o) \neq 0$ and the neighborhood $\mathcal{N}$ is chosen to be small enough, the limit cycle is unique and is attracting if $\sigma_o < 0$ and repelling if $\sigma_o > 0$. We don't prove this here, however.

3. If we adopt the usual convention that $\alpha(\mu_o) = 0$ and $\alpha'(\mu_o) > 0$, i.e., the pair of eigenvalues crosses the imaginary axis from left to right as μ increases beyond μ_o, then remark 2 implies that when $\sigma_o < 0$, an attracting limit cycle exists only when μ lies in the half-open interval $[\mu_o, \mu_o+\varepsilon] \subset \mathcal{N}$. Similarly, when $\sigma_o > 0$, a repelling limit cycle exists only when μ lies in the half-open interval $(\mu_o-\varepsilon, \mu_o] \subset \mathcal{N}$. This property is precisely that depicted in Fig. 2. The sign of σ_o determines whether the limit cycle is attracting (Fig. 2(a)) or repelling (Fig. 2(b)) and is therefore a precise way of saying whether the "bowl" is the right way up, or upside down. This interpretation is in fact the reason for introducing the name "curvature coefficient" for σ_o.

4. An examination of (14) shows that $\sigma_o = 0$ whenever all second and third partial derivatives of $\tilde{f}^1(\underset{\sim}{x},\mu)$ vanish at $\mu = \mu_o$. In this case, either the conclusion of Theorem 1 is still true (non-vanishing higher order derivatives

[5] The reason why we cannot do better and make $\mathcal{R}$ a V contour is that the curve $\dot{V}^{-1}(0)$ need not coincide with some $V^{-1}(\gamma)$: our expression for $\dot{V}$ conceals the fact that if, say, x_1 varies, then the value of γ to make $\dot{V}$ vanish will change slightly.

will be needed) or the conclusion is actually false. An example of the latter case occurs in the van der Pol equation [18-19]:

$$\dot{x}_1 = f_1(x_1,x_2;\mu) = x_2 \qquad (15)$$
$$\dot{x}_2 = f_2(x_1,x_2;\mu) = -\mu(x_1^2-1)x_2 - x_1$$

Equation (15) is already in the standard form with $\mu_o = 0$ as required by (3). Hence $\underset{\sim}{f}(\underset{\sim}{x};\mu) = \tilde{\underset{\sim}{f}}(\underset{\sim}{x};\mu)$. Since all partial derivatives vanish at $\mu = 0$, we have $\sigma_o = 0$ and Theorem 1 says nothing at all. In fact, since it is well known that for arbitrarily small $\mu > 0$, (15) has a stable nearly circular limit cycle of radius 2 [19], it is clear that the van der Pol oscillator works on a mechanism quite different from most nearly sinusoidal electronic oscillators which are designed by implicitly assuming that the oscillator operates as predicted by the Hopf Bifurcation Theorem [1].

2.2. The general case

The Lyapunov function approach can be extended to work for an nth order system but we shall not do so in the present paper because we have already extracted nearly all the geometrical insights it can give. A more elegant proof for $n > 2$ uses the ideas of invariant manifolds; we merely sketch them here and refer the reader to [11,20] for details because an even more appealing proof using frequency-domain concepts will be discussed in the next section.

If one pair of complex conjugate eigenvalues of the Jacobian matrix $\underset{\sim}{J} = (\underset{\sim}{D}\tilde{\underset{\sim}{f}})_{(\underset{\sim}{x};\mu)}$ evaluated at the equilibrium point $\hat{\underset{\sim}{x}}(\mu)$ crosses the imaginary axis as μ varies through μ_o, we might hope that for μ close enough to μ_o, the phenomena of Sec. 2.1 will occur in, or near to, the eigenspace of these eigenvalues, since that eigenspace will be locally invariant under the flow of the differential equation. Proving that this is so is not trivial and in fact requires a rather deep invariant manifold theorem [20]. The following is a simplified but rigorous statement of this theorem in $\mathbb{R}^n$:

Parameterized invariant manifold theorem

Suppose $\mu \in \mathbb{R}$ and $\underset{\sim}{f}(\underset{\sim}{x};\mu)$ is a vector field on $\mathbb{R}^n$, $C^k(k\geq 2)$ jointly in $\underset{\sim}{x}$ and μ and with $\underset{\sim}{f}(\underset{\sim}{0};\mu) = \underset{\sim}{0}$. Let $\underset{\sim}{J}(\mu)$ denote the associated Jacobian matrix evaluated at $\underset{\sim}{x} = \underset{\sim}{0}$. Suppose that for μ in an open neighborhood $\mathcal{N}$ of μ_o, the eigenvalues of $\underset{\sim}{J}(\mu)$ split invariantly into three disjoint sets $\mathcal{S}(\mu)$, $\mathcal{C}(\mu)$, and

$\mathcal{U}(\mu)$, containing s, c, and u eigenvalues, respectively.[6] Assume that all eigenvalues in $\mathcal{S}(\mu)$ have negative real parts, all eigenvalues in $\mathcal{C}(\mu)$ have real parts with the same sign as $\mu - \mu_o$ (and hence are pure imaginary when $\mu=\mu_o$), and all eigenvalues in $\mathcal{U}(\mu)$ have positive real parts. Let $W^s(\mu)$, $W^c(\mu)$, and $W^u(\mu)$ be the eigenspaces of $\underset{\sim}{J}(\mu)$ corresponding to the eigenvalues in $\mathcal{S}(\mu)$, $\mathcal{C}(\mu)$, and $\mathcal{U}(\mu)$, respectively, and suppose

$$\mathbb{R}^n = W^s(\mu) \oplus W^c(\mu) \oplus W^u(\mu)$$

for all $\mu \in \mathcal{N}$

Then there exist 3 families (parameterized by μ) of differentiable manifolds $\mathcal{M}^s(\mu)$, $\mathcal{M}^c(\mu)$ and $\mathcal{M}^u(\mu)$ which are defined on an open neighborhood $\mathcal{P}$ of $\underset{\sim}{0}$ in $\mathbb{R}^n$ for all $\mu \in \mathcal{N}$; namely,

$$\mathcal{M}^\ell(\mu) = \{\underset{\sim}{x}: \ \underset{\sim}{m}^\ell(\underset{\sim}{x};\mu)=\underset{\sim}{0}\}$$

where $\underset{\sim}{m}^\ell$: $\mathcal{P} \times \mathcal{N} \to \mathbb{R}^{n-\ell}$ is a C^k function, for ℓ = s, c, or u. These manifolds intersect only at the origin and are invariant under the flow of the vector field $\underset{\sim}{f}$ restricted to $\mathcal{P} \times \mathcal{N}$.[7]

Furthermore, at $\underset{\sim}{x} = \underset{\sim}{0}$, each manifold $\mathcal{M}^\ell(\mu)$ is tangent at the origin to the associated eigenspace $W^\ell(\mu)$.

Remark.

Although the stable manifold $\mathcal{M}^s(\mu)$ and the unstable manifold $\mathcal{M}^u(\mu)$ are uniquely defined, the center manifold $\mathcal{M}^c(\mu)$ is not necessarily unique. However, it can be shown that any center manifold does contain all the local recurrence of trajectories [10]. Also, $\mathcal{M}^c(\mu)$ depends in a C^k way on μ because $\underset{\sim}{m}^c$ is C^k and the Jacobian matrix of $\underset{\sim}{m}^c$ evaluated at $\underset{\sim}{x} = \underset{\sim}{0}$ is invertible on W^c so that we can apply the inverse function theorem.

With the help of the invariant manifold theorem, it is now easy to prove the existence of closed orbits for an nth order system having only one pair of

---

[6] By invariant, we mean here that if an eigenvalue λ belongs to $\mathcal{S}$, $\mathcal{C}$, or $\mathcal{U}$ for some $\mu \in \mathcal{N}$, then the locus of $\lambda(\mu)$ remains in the same set $\mathcal{S}$, $\mathcal{C}$, or $\mathcal{U}$, as μ varies over the neighborhood $\mathcal{N}$. The notations "s", "c", and "u" denote stable, center, and unstable, respectively.

[7] Restating this in more geometrical terms, it means that if $\underset{\sim}{x}_o \in \mathcal{N}$ lies on any one of the 3 manifolds, the trajectory of the differential equation $\dot{\underset{\sim}{x}} = \underset{\sim}{f}(\underset{\sim}{x};\mu)$ passing through $\underset{\sim}{x}_o$ must lie on the same manifold for all times where it remains within $\mathcal{N}$.

complex conjugate eigenvalues which crosses the imaginary axis as μ varies through μ_o. In this case, the center manifold is 2-dimensional and hence its vector field is topologically equivalent to a vector field on $\mathbb{R}^2$. Hence we can simply invoke Theorem 1 from Sec. 2.1 to assert the existence of a periodic orbit lying entirely in $\mathcal{M}^c(\mu)$. Since $\mathcal{M}^c(\mu) \subset \mathbb{R}^n$, this implies the existence of at least one periodic orbit in $\mathbb{R}^n$. Pictorially, what we are doing here is to stretch the 2-dimensional surface $\mathcal{M}^c(\mu)$ as if it were a rubber sheet and then flatten it into a plane. Clearly, the resulting phase portrait is merely distorted: its qualitative behavior remains unchanged. This proof can be made completely rigorous by taking a local chart for $\mathcal{M}^c(\mu)$ (i.e., a smooth bijective mapping of $\mathcal{M}^c(\mu)$ onto a subset of $\mathbb{R}^2$) and then applying Theorem 1.

That there exists a unique periodic orbit in $\mathcal{P} \subset \mathbb{R}^n$ for each $\mu \in \mathcal{N}$ is also not difficult to prove (assuming we have proved it in $\mathbb{R}^2$) as long as all of the other eigenvalues of $\underset{\sim}{J}(\mu)$ are clear of the imaginary axis so that only one pair of complex conjugate eigenvalues crosses it at $\mu = \mu_o$.

Stability requires extra work. First, we have to make sure that the center manifold is itself attracting for there to be any chance of the periodic orbit being attracting. Second, the fact that the vague attractor condition involves second and third partial derivatives of the restriction of $\underset{\sim}{f}(\underset{\sim}{x};\mu)$ to $\mathcal{M}^c(\mu)$ means that the curvature of $\mathcal{M}^c$ will affect the formula for a corresponding generalized curvature coefficient σ_o. Given that the invariant manifold theorem has been developed properly, however, the new formula for σ_o comes out without too much extra work. See [10] for details. Since we shall be using a more convenient but equivalent formula in Sec. 3.6, we do not give the extra terms required in the following theorem.

We will close this section by stating the complete Hopf bifurcation theorem in $\mathbb{R}^n$. It is essentially taken from [10] (see also [8]). The requirement that f be C^4 is clear in view of the need for error terms to be $O(|\underset{\sim}{x}|^4)$ when we were computing σ_o in Sec. 2.1.

Theorem 2. Time-domain Hopf bifurcation theorem in $\mathbb{R}^n$

Let $\dot{\underset{\sim}{x}} = \underset{\sim}{f}(\underset{\sim}{x};\mu)$ be an nth order system ($n \geq 2$) parameterized by $\mu \in \mathbb{R}$ and C^4 jointly in $\mu \in \mathbb{R}$ and $\underset{\sim}{x} \in \mathbb{R}^n$. Let $\underset{\sim}{f}\left(\hat{\underset{\sim}{x}}(\mu);\mu\right) = \underset{\sim}{0}$ for a locally unique equilibrium point $\hat{\underset{\sim}{x}}(\mu)$ and write $\underset{\sim}{J}(\mu)$ for the Jacobian matrix of $\underset{\sim}{f}$ evaluated at $\hat{\underset{\sim}{x}}(\mu)$. Suppose:

(1) $\underset{\sim}{J}(\mu)$ has a pair of simple complex-conjugate eigenvalues $\lambda(\mu) = \alpha(\mu) + i\omega(\mu)$ and $\bar{\lambda}(\mu) = \alpha(\mu) - i\omega(\mu)$, where $\alpha(\mu) = 0$ at $\mu = \mu_o$ and $\alpha'(\mu_o) > 0$.

(2) Every other eigenvalue $\nu(\mu)$ of $J(\mu)$ satisfies Re $\nu(\mu_o) \neq 0$.

(3) $\sigma_o \neq 0$ where σ_o is defined by (51) of Sec. 3.3 (or by (14) if n = 2).

Then there is an open neighborhood $\mathcal{N}$ of μ_o and for each $\mu \in \mathcal{N}$, there is an open neighborhood $\mathcal{O}$ of $\hat{x}(\mu)$ of size $\varepsilon = O\left(|\alpha(\mu)|^{1/2}\right)$ such that the following statements are true:

(a) If $\alpha(\mu)\sigma_o < 0$, there is a unique periodic orbit in $\mathcal{O}$. For μ sufficiently close to μ_o, the time waveform corresponding to this periodic orbit is almost sinusoidal with an angular frequency $\omega(\mu_o)/2\pi + O(|\alpha(\mu)|)$ and an amplitude which grows at the same rate as $\sqrt{|\mu-\mu_o|}$.

(b) If $\sigma_o < 0$ and Re $\nu(\mu_o) < 0$ for all eigenvalues ν other than $\lambda(\mu_o)$ and $\bar{\lambda}(\mu_o)$, then this periodic orbit is attracting.

(c) If $\sigma_o > 0$ and Re $\nu(\mu_o) > 0$ for all eigenvalues ν other than $\lambda(\mu_o)$ and $\bar{\lambda}(\mu_o)$, then this periodic orbit is repelling.

3. The Hopf Bifurcation in the Frequency Domain

3.1. Assumptions for the frequency-domain Hopf bifurcation theorem

Although Sec. 2 has given us a very clear time-domain picture of what is happening in the Hopf bifurcation, we have not yet provided a complete proof of this theorem. Also, the invariant manifold theorem -- a key step required in the time-domain proof -- has been merely stated because its proof is fairly long and would not help us much in understanding the Hopf bifurcation. Our objective in this section is to show that a self-contained frequency-domain proof of the complete Hopf bifurcation theorem can be produced quite independently of the invariant manifold theory. This proof is due to Allwright [14] and although our development is slightly different, we shall refer to results in his paper at certain vital points.

Allwright's proof has several advantages and is particularly attractive if one is interested in feedback systems. First, it uses harmonic balance (describing function) methods which are well-known to circuit and control engineers. Second, Allwright gave a very useful graphical interpretation for single-loop systems. We shall show how to extend his interpretation to multiple-loop systems and so provide a completely general graphical method in the frequency domain reminiscent of the Nyquist criterion. Third, even when there are many feedback loops, Allwright's formula for calculating the curvature coefficient in the frequency domain is never harder and is usually much easier to use than the corresponding time-domain formula given by Marsden and McCracken. Fourth, the frequency-domain version of the theorem can be easily

extended to allow delays and other distributed elements such as transmission lines. A corresponding time-domain proof for the infinite-dimensional case would have been much more involved.

Suppose, then, that we have a standard form autonomous multiple-loop feedback system which has been separated into a dynamical linear part with a transfer matrix $\underset{\sim}{G}$ and a memoryless nonlinear part $\underset{\sim}{f}$, as shown in Fig. 3(a).[8] For complete generality, we assume that G has "ℓ" inputs and "m" outputs where ℓ need not be equal to m. Hence, $\underset{\sim}{f}$ maps $\mathbb{R}^m$ into $\mathbb{R}^\ell$ and $\underset{\sim}{G}$ is an $m\times\ell$ matrix. Both $\underset{\sim}{G}$ and $\underset{\sim}{f}$ may depend on μ. The elements of $\underset{\sim}{G}$ need not be rational functions of s, so we are allowing linear distributed parameter systems. Observe that our feedback representation in Fig. 3(a) is extremely general and automatically includes all lumped autonomous systems. In particular, consider the general ordinary differential equation.

$$\boxed{\dot{\underset{\sim}{x}} = \underset{\sim\sim}{A}\underset{\sim}{x} + \underset{\sim}{B}\,\underset{\sim}{g}(\underset{\sim\sim}{C}\underset{\sim}{x};\mu)} \tag{16}$$

where $\underset{\sim\sim}{A}$ is an nxn matrix, $\underset{\sim}{B}$ is an $n\times\ell$ matrix, $\underset{\sim\sim}{C}$ is an mxn matrix, and $\underset{\sim}{g}: \mathbb{R}^m \to \mathbb{R}^\ell$. All three matrices may depend on μ, and $\underset{\sim\sim}{A}$ may be the zero matrix.
The autonomous system $\dot{\underset{\sim}{x}} = \underset{\sim}{f}(\underset{\sim}{x};\mu)$ is a special case of (16) where $\underset{\sim\sim}{A} = \underset{\sim\sim}{0}$, $\underset{\sim}{B} = \underset{\sim\sim}{C} = \underset{\sim\sim}{1}$, and $\underset{\sim}{f} = \underset{\sim}{g}$. We will now show that given (16), there corresponds an infinitely many distinct but equivalent feedback representations.[9] To do this, let us introduce an arbitrary nxm matrix $\underset{\sim\sim}{D}$ (which may depend on μ) and rewrite (16) as follows:

$$\dot{\underset{\sim}{x}} = \underset{\sim\sim}{A}\underset{\sim}{x} + \underset{\sim\sim}{B}\underset{\sim\sim}{D}\underset{\sim}{y} + \underset{\sim}{B}\left[\underset{\sim}{g}(\underset{\sim}{y};\mu) - \underset{\sim\sim}{D}\underset{\sim}{y}\right] \tag{17}$$

where

$$\underset{\sim}{y} = \underset{\sim\sim}{C}\underset{\sim}{x} \tag{18}$$

---

[8] Because $\underset{\sim}{G}$ is linear, the negative sign can appear at any point in the loop. With the form shown, we are thinking of $\underset{\sim}{G}$ as a system to be controlled and $\underset{\sim}{f}$ as the controller, so $\underset{\sim}{e}$ in Fig. 3(a) is the error signal and $\underset{\sim}{d}$ (=$\underset{\sim}{0}$, here) is the desired behavior. The results still hold, however, if we transfer the negative sign to the other side of $\underset{\sim}{G}$.

[9] The following formulation is standard but seems not to be well known.

Taking the Laplace transform $\mathcal{L}$ of both sides and solving for $\mathcal{L}\underset{\sim}{x}$ as a function of the Laplace variable s, then writing $\underset{\sim}{e} = -\underset{\sim}{C}\underset{\sim}{x}$, we obtain

$$(\mathcal{L}\underset{\sim}{e})(s) = -\underset{\sim}{G}(s;\mu)(\mathcal{L}\underset{\sim}{u})(s) \tag{19a}$$

where

$$\underset{\sim}{G}(s;\mu) = \underset{\sim}{C}[s\,\underset{\sim}{1} - (\underset{\sim}{A}+\underset{\sim}{B}\underset{\sim}{D}\underset{\sim}{C})]^{-1}\underset{\sim}{B} \tag{19b}$$

$$\underset{\sim}{u} = \underset{\sim}{f}(e;\mu) \triangleq \underset{\sim}{g}(\underset{\sim}{y};\mu) - \underset{\sim}{D}\underset{\sim}{y} \tag{19c}$$

$$\underset{\sim}{y} = -\underset{\sim}{e} \tag{19d}$$

It follows from (19) that the autonomous system (16) is equivalent to the feedback system shown in Fig. 3(a), provided $\underset{\sim}{G}$ and $\underset{\sim}{f}$ are defined by (19b) and(19c), respectively. Since the matrix $\underset{\sim}{D}$ is arbitrary, we have in fact produced a continuum of equivalent feedback system representations. In practice, we will usually choose $\underset{\sim}{D} = \underset{\sim}{0}$ if $\underset{\sim}{A} \neq \underset{\sim}{0}$, and $\underset{\sim}{D} = \underset{\sim}{1}$ if $\underset{\sim}{A} = \underset{\sim}{0}$.

Observe that even though (16) is an n-dimensional system, the nonlinear function $f: \mathbb{R}^m \to \mathbb{R}^\ell$ is an ℓ-dimensional vector. Since "ℓ" is never greater than "n" in (16),[10] and in practice is usually much smaller, it is reasonable to expect that the frequency-domain version of the Hopf theorem would usually require much less computation than its time-domain counterpart. For example, the equilibrium point $\hat{\underset{\sim}{x}}(\mu)$ obtained by setting $\dot{\underset{\sim}{x}} = \underset{\sim}{0}$ in (16) and solving the resulting system of "m" nonlinear equations, now corresponds to the point $\hat{\underset{\sim}{e}}(\mu)$ obtained by setting s = 0 in (19b) and solving the following system of "ℓ" nonlinear equations:

$$\boxed{\underset{\sim}{G}(0;\mu)\underset{\sim}{f}(\underset{\sim}{e};\mu) = -\underset{\sim}{e}} \tag{20}$$

If we linearize the feedback system in Fig. 3(a) about the equilibrium point $\hat{\underset{\sim}{e}}(\mu)$, we obtain the system shown in Fig. 3(b). It follows from feedback system theory that if an eigenvalue of the Jacobian matrix associated with (16) assumes the pure imaginary value $i\omega_o$ at $\mu = \mu_o$, then a corresponding eigenvalue of the open-loop matrix $\underset{\sim}{G}(i\omega_o,\mu_o)\ \underset{\sim}{J}(\mu_o)$ associated with the feedback system (19) must assume the value -1 + i0 at $\mu = \mu_o$. Hence, instead of assuming that a simple pair of eigenvalues are equal to $\pm i\omega_o$ at $\mu = \mu_o$ (condition (1) of Theorem 2) as in the time-domain Hopf theorem, we must now assume that $\underset{\sim}{G}(i\omega_o;\mu_o)\ \underset{\sim}{J}(\mu_o)$ has <u>exactly one</u> eigenvalue equal to -1 + i0 for the frequency-domain Hopf theorem.

[10] Otherwise, we can always replace $\underset{\sim}{B}\underset{\sim}{g}(\underset{\sim}{C}\underset{\sim}{x};\mu)$ by $\hat{\underset{\sim}{B}}\hat{\underset{\sim}{g}}(\underset{\sim}{C}\underset{\sim}{x};\mu)$ where $\hat{\underset{\sim}{B}} = \underset{\sim}{1}$.

At this point we must very briefly summarize the frequency domain approach to linear multivariable system stability. Suppose we fix a value of μ and temporarily write $\underset{\sim}{G}(i\omega)$ instead of $\underset{\sim}{G}(i\omega;\mu)$. The square matrix $\underset{\sim}{G}(i\omega)\underset{\sim}{J}$ has m eigenvalues which depend on ω, but this does not mean that one can define m functions $\lambda_j(i\omega)$, $j = 1,2,\ldots,m$. In fact, the characteristic equation of $\underset{\sim}{G}(i\omega)\underset{\sim}{J}$ is a polynomial of mth order in λ, with coefficients which are functions of $i\omega$. If $\underset{\sim}{G}(s)$ has elements which are rational functions of s, the coefficients in the characteristic equation can be made into polynomials in s by multiplying by the least common denominator, and λ is an algebraic function of s, defined on a Riemann surface in general [15]. (Even if the elements of $\underset{\sim}{G}(s)$ are not rational functions the stability criterion which follows is true [21], but we shall take the simplest case.) The algebraic function will have a number of components which correspond roughly to the λ_j we would like to define, but if λ has any branch points, some components will be defined on a Riemann surface with several sheets and will each represent several of the λ_j. However, the argument principle, on which the single loop Nyquist stability criterion depends, remains true for functions defined on Riemann surfaces [27]. This allows one to build up a theory completely analogous to the single loop theory based on counting encirclements of the point -1 by the Nyquist locus [15].

The end result is that one simply calculates all the eigenvalues at some ω, then repeats this at $\omega + \delta\omega$ and so on through $[0,\omega)$. The points are joined up smoothly to give the characteristic loci; any ambiguities in joining up are genuine and arise from the nature of the algebraic function, but will not affect the stability test. Next, the total number of anticlockwise encirclements of $-1 + i0$ by the loci is counted: if it is equal to the number of poles of $\lambda(s)$ with real part positive,[11] the system is stable. (This counting method is just a convenient way of determining whether 0 is in the image of the right half s-plane under the map $\det(\underset{\sim}{G}(s)\underset{\sim}{J}+\underset{\sim}{1})$.)

Notice that we are already in a position to check most of the hypotheses of the Hopf theorem: if some component of the characteristic loci moves through $-1 + i0$ as μ varies, and if the value of ω for which an eigenvalue is $-1 + i0$ is itself nonzero, we have a pair of eigenvalues of the linearized time domain equations crossing the imaginary axis. The condition that this should happen for some ω and not for integers $r\omega$ ($r \neq \pm 1$) can be checked by ensuring that at

[11] Poles of $\lambda(s)$ are zeros of the coefficient of λ^m in the characteristic polynomial defining λ.

the critical μ value, no other component or other part of the same component, should pass through $-1 + i0$ with the relevant frequency: this will generally be obvious from a glance at the diagram, but we shall impose a stronger condition in the theorem which ensures that there is no resonance.

3.2. The graphical Hopf theorem

We shall state and prove a theorem which not only shows how to check the eigenvalue conditions using characteristic loci but also incorporates a check of the sign of σ_o into the same diagram. It will enable us to provide estimates of the frequency and amplitude of the limit cycle correct up to $O(|\mu-\mu_o|)$, the error in frequency being $O(|\mu-\mu_o|^2)$ and that in amplitude being $O(|\mu-\mu_o|^{3/2})$. These will be read directly from our diagram, but in Sec. 3.3, we shall show how to use the more usual approach of calculating first approximations and then correction terms. In fact, the parameter μ plays almost no role in the theorem and it can be suppressed at little cost. Its place will be taken by a parameter θ which is essentially the amplitude, so $\theta = O(|\mu-\mu_o|^{1/2})$. Although the statement is lengthy because we have to take care over orders of magnitude, the theorem is very easy to use in practice. The statement of the Theorem and the remarks which follow it should be sufficient for practical use, without the need to refer to the Lemmas which are used in the proof.

Theorem 3 (Graphical Hopf)

Let S be a feedback system of the form in Fig. 3(a) and which is equivalent to a differential equation $\mathcal{D}$ of the form (16), and suppose $\underset{\sim}{f}: \mathbb{R}^m \to \mathbb{R}^\ell$ is C^4. Suppose $\hat{\underset{\sim}{e}}$ is a locally unique solution of $\underset{\sim}{G}(0)\underset{\sim}{f}(\underset{\sim}{e}) + \underset{\sim}{e} = \underset{\sim}{0}$ and write $\underset{\sim}{J} = (D\underset{\sim}{f})_{\hat{\underset{\sim}{e}}}$. Write $\hat{\underset{\sim}{x}}$ for the corresponding equilibrium of the differential equation.

Let $\underset{\sim}{G}(s)\underset{\sim}{J}$ have characteristic function $\lambda(s)$ and let $\hat{\lambda}$ be the component of λ corresponding to the branch of the characteristic locus which intersects the negative real axis closest to $-1 + i0$, the intersection being at $\hat{\lambda}(i\omega_R)$.

Suppose $\zeta(\omega_R)$ as found from Table 2 is nonzero and the half-line from -1 in the direction defined by $\zeta(\omega_R)$ first intersects the locus of $\hat{\lambda}(i\omega)$ at $\hat{P}$, with $\hat{\lambda}(i\hat{\omega}) = \hat{P} = -1 + \hat{\theta}^2\zeta(\omega_R)$, where $\hat{\theta} \geq 0$. (See Fig. 4.)

If (i) the intersection is transversal

and (ii) there are no other intersections between the characteristic loci and the closed line segment joining $-1 + i0$ to $\hat{P}$

then there exist $\theta_o \geq \theta_1 > 0$ and $\omega_o \geq \omega_1 > 0$ such that

(a) if $\hat{\theta} < \theta_o$ and $|\omega-\omega_R| < \omega_o$ the system S has a periodic solution $\underset{\sim}{e}(t)$

of frequency $\omega = \hat{\omega} + O(\hat{\theta}^4)$ and such that $\underset{\sim}{e}(t) = \hat{\underset{\sim}{e}} + \sum_{k=-2}^{2} \underset{\sim}{E}^k \exp ik\omega t + O(\hat{\theta}^3)$ where $\underset{\sim}{E}^k$ $(k=0,\pm1,\pm2)$ will be defined later.

(b) The corresponding limit cycle in $\mathcal{D}$ is unique in a ball centered on $\hat{\underset{\sim}{x}}$ and of radius O(1). If $\hat{\theta} < \theta_1$ and $|\omega-\omega_R| < \omega_1$, the limit cycle is the unique attractor in a ball centered on $\hat{\underset{\sim}{x}}$ and of radius O(1) if the following encirclement condition holds: The total number of anticlockwise encirclements of $\hat{P} + \zeta\delta$ by all the branches of λ is equal to the number of poles of λ with positive real part. Here $\delta > 0$ is so small that no new intersections between the locus and the half-line are introduced.

Remarks

1. The need for ω_o and ω_1 arises because by locating the intersection as in Fig. 4 we have solved the equation $\hat{\lambda}(i\omega) + 1 = \theta^2\zeta(\omega)$ approximately. Doing so does not change the order of magnitude of the error (see Lemma 3.1).
2. θ essentially replaces μ as the parameter. If one is interested in several μ values, the picture will usually have to be redrawn each time.
3. A transversal intersection is one at which the intersecting curves are not parallel and have nonzero rates of change with respect to their parameterizations. Here, this means that

$$\det \begin{bmatrix} \text{Re } \zeta & \text{Im } \zeta \\ \text{Re } \hat{\lambda}'(i\omega) & \text{Im } \hat{\lambda}'(i\omega) \end{bmatrix} \neq 0$$

but one can check the condition immediately by looking at the diagram.

4. The encirclement condition in (b) is the familiar Nyquist stability criterion, with the critical point moved from -1 to a point just "beyond" $\hat{P}$, where "beyond" means we increase θ slightly from $\hat{\theta}$. This condition is similar to an approximate one often used with describing functions, but in the present case it is rigorous.

   Usually $\underset{\sim}{G}(s)\underset{\sim}{J}$ (hence $\lambda(s)$) will have no poles in the right half plane and the -1 point will not be encircled except by $\hat{\lambda}$. Then the condition is simply that the half-line should point outwards at the intersection $\hat{P}$ for the limit cycle to be attracting.

5. The stability result can be understood very easily in the light of Sec. 2. The encirclement conditions check whether all but two eigenvalues of the original differential equations have negative real part, so that the center manifold is attracting. The condition on the $\hat{\lambda}$ branch determines whether the solution exists while the equilibrium is stable (subcritical bifurcation:

unstable limit cycle) or while the equilibrium is unstable (Supercritical bifurcation: stable limit cycle). However, Allwright's proof of stability is independent of these considerations, and hence does not require us to prove the center manifold theorem.

6. We have imposed stronger conditions than necessary in several places, in order to simplify the statement of the theorem. In particular, we have assumed the state space is finite dimensional so $\underset{\sim}{G}$ is rational. However, the generalization of most of the theorem to the distributed case is simple and it is only because of certain complications in the graphical interpretation that we do not give it here.

To prove the theorem we shall need a number of Lemmas.

Lemma 3.1. (Justification of approximate graphical solution)

Under condition (i) of Theorem 3, for any $\varepsilon > 0$ there is an $\omega_\varepsilon > 0$ and a $\theta_\varepsilon > 0$ such that if $|\hat{\omega}-\omega_R| < \omega_\varepsilon$ and $\hat{\theta} < \theta_\varepsilon$, there is a unique solution $(\tilde{\omega},\tilde{\theta})$ to

$$\hat{\lambda}(i\omega) + 1 = \theta^2(\zeta(\omega)+\rho(\theta,\omega)) \tag{21}$$

where ρ is a C^1 function which is $O(\theta)$ for all ω. Moreover, $\tilde{\omega} = \hat{\omega} + d_1(\theta,\omega)$ and $\tilde{\theta} = \hat{\theta} + d_2(\theta,\omega)$ where d_1, d_2 are C^1 functions and $|d_1| < \varepsilon$, $|d_2| < \varepsilon$.

Proof. This is just a slightly modified implicit function theorem. The transversality condition ensures that if we regard the complex plane as $\mathbb{R}^2$ and think of

$$\hat{\lambda}(i\omega) + 1 - \theta^2\zeta(\omega_R) \tag{22}$$

as a map from a neighborhood of $(\hat{\theta}^2,\hat{\omega})$ to $\mathbb{R}^2$, this map has a nonsingular derivative $\underset{\sim}{\Gamma}$ at $(\hat{\theta}^2,\hat{\omega})$. Consequently, the modified Newton-Raphson map $\underset{\sim}{M}$: $\mathbb{R}^2 \to \mathbb{R}^2$ defined by

$$(\theta^2,\omega) \overset{\underset{\sim}{M}}{\mapsto} (\theta^2,\omega) - \Gamma^{-1}\left\{\hat{\lambda}(i\omega) + 1 - \theta^2(\zeta(\omega)+\rho(\theta,\omega))\right\} \tag{23}$$

is a contraction on a closed set Ω containing $(\hat{\theta}^2,\hat{\omega})$ if $|\hat{\omega}-\omega_R|$ and $\hat{\theta}$ are sufficiently small, as we now show. Let us first rewrite (23) as follows:

$$\underset{\sim}{M}(\theta^2,\omega) = (\theta^2,\omega) - \Gamma^{-1}\left\{[\hat{\lambda}(i\omega)+1-\theta^2\zeta(\omega_R)] + \theta^2[\zeta(\omega_R)-\zeta(\omega)-\rho(\theta,\omega)]\right\} \tag{24}$$

Recalling that $\underset{\sim}{\Gamma}$ is the derivative of (22), we obtain the following derivative of $\underset{\sim}{M}$:

$$\begin{aligned}(\underset{\sim}{DM})_{(\theta^2,\omega)} &= \underset{\sim}{1} - \underset{\sim}{\Gamma}^{-1}\left\{\underset{\sim}{\Gamma}+\underset{\sim}{D}[\theta^2(\zeta(\omega_R)-\zeta(\omega)-\rho(\theta,\omega))]\right\} \\ &= \underset{\sim}{\Gamma}^{-1}\underset{\sim}{D}[\theta^2(\zeta(\omega_R)-\zeta(\omega)-\rho(\theta,\omega))]\end{aligned} \tag{25}$$

where $\underset{\sim}{D}$ denotes the derivative operator. Since ζ and ρ are C^1 functions of ω and θ^2, it follows from (25) that

$$\|\underset{\sim}{D}\underset{\sim}{M}\| \leq K|(\theta^2,\omega-\omega_R)| \tag{26}$$

on a closed set Ω containing $(\hat{\theta}^2,\hat{\omega})$, where K is a constant, $|\cdot|$ is the Euclidean norm on (θ^2,ω) space and $\|.\|$ is the induced matrix norm. Thus if θ and $|\omega-\omega_R|$ are sufficiently small, $\underset{\sim}{M}$ has Lipschitz constant less than 1. Next, we show that $\underset{\sim}{M}$ maps Ω into itself if θ and $|\omega-\omega_R|$ are sufficiently small. Since, using (22) and (24), we have

$$\underset{\sim}{M}(\theta^2,\omega) - (\hat{\theta}^2,\hat{\omega}) = \underset{\sim}{M}(\theta^2,\omega) - \underset{\sim}{M}(\hat{\theta}^2,\hat{\omega}) + \underset{\sim}{\Gamma}^{-1}\hat{\theta}^2[\zeta(\omega_R)-\zeta(\hat{\omega})-\rho(\hat{\theta},\hat{\omega})] \tag{27}$$

and the right side is $O(\theta^3,\theta^2(\omega-\hat{\omega}),(\omega-\hat{\omega})^2)$ which implies that $\underset{\sim}{M}(\theta^2,\omega)$ is closer to $(\hat{\theta}^2,\hat{\omega})$ than was (θ^2,ω), for every (θ^2,ω) within some fixed distance of $(\hat{\theta}^2,\hat{\omega})$. The Lemma now follows at once from the contraction mapping theorem. ¤

Remarks. We shall use this type of argument several times and from now on we shall suppress the details. Condition (ii) of Theorem 3 is not needed directly in this Lemma, but it is useful in excluding cases where $|\omega-\omega_R|$ is clearly too large.

Lemma 3.2. (Relation between graphical and second order harmonic balance solution)

Under conditions (i) and (ii) of the Theorem, the solution $(\hat{\omega},\hat{\theta})$ of $\hat{\lambda}(i\omega) + 1 = \theta^2\zeta(\omega_R)$ corresponds to a locally unique second order harmonic balance solution for a limit cycle in the system provided $\hat{\theta}$ is sufficiently small.

Remark. The frequency and amplitude vectors will be found during the proof. This result, together with the next Lemma which asserts that the harmonic balance solution is close to a true solution, gives the required approximation to the limit cycle.

Proof. A second order harmonic balance solution has the form

$$\underset{\sim}{e}(t) = \hat{\underset{\sim}{e}} + \sum_{k=-2}^{2} \underset{\sim}{E}^k \exp ik\omega t \tag{28}$$

Here the phase of one component of, say $\underset{\sim}{E}^1$ can be chosen arbitrarily by shifting the time origin. Since $\underset{\sim}{e}(t)$ has frequency ω, so does $\underset{\sim}{f}(\underset{\sim}{e}(t))$ and we can calculate its Fourier coefficients $\underset{\sim}{F}^k$ as functions of $\underset{\sim}{E}^0$, $\underset{\sim}{E}^{\pm 1}$, $\underset{\sim}{E}^{\pm 2}$.

Equating the input and output of the linear part gives

$$\underset{\sim}{E}^k = -\underset{\sim}{G}(ik\omega)\underset{\sim}{F}^k \tag{29}$$

and we wish to solve this when $k = 0, \pm 1, \pm 2$. Clearly, $\underset{\sim}{E}^{-k} = \bar{\underset{\sim}{E}}^k$, where the

"bar" denotes complex conjugation. It is convenient to solve first for $\underset{\sim}{E}^0$ and $\underset{\sim}{E}^2$ in terms of $\underset{\sim}{E}^1$. By expanding $\underset{\sim}{f}(\underset{\sim}{e})$ in a Taylor series about $\hat{\underset{\sim}{e}}$ and substituting the trial expression for $\underset{\sim}{e}$ it is simple to verify that

$$\underset{\sim}{F}^0 = (\underset{\sim}{D}\underset{\sim}{f})_{\hat{\underset{\sim}{e}}}\underset{\sim}{E}^0 + \frac{1}{4}(\underset{\sim}{D}^2\underset{\sim}{f})_{\hat{\underset{\sim}{e}}}\underset{\sim}{E}^1 \otimes \bar{\underset{\sim}{E}}^1 + \underset{\sim}{\rho}_1 \tag{30}$$

$$\underset{\sim}{F}^2 = (\underset{\sim}{D}\underset{\sim}{f})_{\hat{\underset{\sim}{e}}}\underset{\sim}{E}^2 + \frac{1}{4}(\underset{\sim}{D}^2\underset{\sim}{f})_{\hat{\underset{\sim}{e}}}\underset{\sim}{E}^1 \otimes \underset{\sim}{E}^1 + \underset{\sim}{\rho}_2 \tag{31}$$

where $\underset{\sim}{\rho}_1$ and $\underset{\sim}{\rho}_2$ are quartic in $|\underset{\sim}{E}^1|$ and quadratic in $|\underset{\sim}{E}^0|$ and $|\underset{\sim}{E}^2|$. Here $\otimes$ is the tensor product operator [28], so for example the second term in the $\underset{\sim}{F}^0$ expression has kth component $\sum_{r,s=1}^{m} f^k_{rs} E^1_r \bar{E}^1_s$ in the notation used for derivatives in Sec. 2.

Writing $\underset{\sim}{J}$ for $(\underset{\sim}{D}\underset{\sim}{f})_{\hat{\underset{\sim}{e}}}$, $\underset{\sim}{Q}$ for $(\underset{\sim}{D}^2\underset{\sim}{f})_{\hat{\underset{\sim}{e}}}\underset{\sim}{E}^1$, and $\underset{\sim}{H}$ for the closed loop transfer function from $\underset{\sim}{v}$ to $\underset{\sim}{y}$ of the linearized feedback loop in Fig. 3(b), so

$$\underset{\sim}{H}(s) = (\underset{\sim}{G}(s)\underset{\sim}{J}+\underset{\sim}{1})^{-1}\underset{\sim}{G}(s) \tag{32}$$

we have

$$\boxed{\underset{\sim}{E}^0 = -\underset{\sim}{H}(0)\ \frac{1}{4}\underset{\sim}{Q}\bar{\underset{\sim}{E}}^1 + O(|\underset{\sim}{E}^1|^4)} \tag{33}$$

$$\boxed{\underset{\sim}{E}^2 = -\underset{\sim}{H}(2i\omega)\ \frac{1}{4}\underset{\sim}{Q}\underset{\sim}{E}^1 + O(|\underset{\sim}{E}^1|^4)} \tag{34}$$

where we have suppressed an implicit function theorem argument of the type used in Lemma 3.1 and have used condition (ii) to ensure that $\underset{\sim}{G}(s)\underset{\sim}{J} + \underset{\sim}{1}$ is invertible when $s = 0$ and $s = 2i\omega$. Note that $\underset{\sim}{E}^0$ and $\underset{\sim}{E}^2$ are $O(|\underset{\sim}{E}^1|^2)$.

The equation for $\underset{\sim}{F}^1$ is

$$\underset{\sim}{F}^1 = (\underset{\sim}{D}\underset{\sim}{f})\underset{\sim}{E}^1 + (\underset{\sim}{D}^2\underset{\sim}{f})[\underset{\sim}{E}^0 \otimes \underset{\sim}{E}^1 + \bar{\underset{\sim}{E}}^1 \otimes \underset{\sim}{E}^2] + \frac{1}{8}(\underset{\sim}{D}^3\underset{\sim}{f})\underset{\sim}{E}^1 \otimes \underset{\sim}{E}^1 \otimes \bar{\underset{\sim}{E}}^1 + \underset{\sim}{\rho}_3 \tag{35}$$

where $\underset{\sim}{\rho}_3$ is, after substituting (33) and (34), $O(|\underset{\sim}{E}^1|^4)$. Thus we have to solve

$$\boxed{[\underset{\sim}{G}(i\omega)\underset{\sim}{J}+\underset{\sim}{1}]\underset{\sim}{E}^1 = -\underset{\sim}{G}(i\omega)\underset{\sim}{p}(\omega,\underset{\sim}{E}^1)} \tag{36}$$

where

$$\underset{\sim}{p} = \underset{\sim}{Q}\underset{\sim}{E}^0 + \frac{1}{2}\bar{\underset{\sim}{Q}}\underset{\sim}{E}^2 + \frac{1}{8}\underset{\sim}{L}\bar{\underset{\sim}{E}}^1 + O(|\underset{\sim}{E}^1|^4) \tag{37}$$

and

$$\underset{\sim}{L} = (\underset{\sim}{D}^3\underset{\sim}{f})_{\hat{\underset{\sim}{e}}}\underset{\sim}{E}^1 \otimes \underset{\sim}{E}^1. \tag{38}$$

Thus after substitution of (33) and (34), $\underset{\sim}{p}$ only depends on ω and $|\underset{\sim}{E}^1|$ and is third order in $|\underset{\sim}{E}^1|$.

The matrix multiplying $\underset{\sim}{E}^1$ on the left side of (36) is singular at bifurcation so we cannot solve directly. Instead, we notice that since we are looking for small $\underset{\sim}{E}^1$ the left side, being first order, would be expected to

dominate; so $\underset{\sim}{E}^1$ should be nearly an eigenvector of $\underset{\sim}{G}(i\omega)\underset{\sim}{J}$ belonging to the eigenvalue $\hat{\lambda}(i\omega)$ which is -1 at bifurcation. This suggests we try

$$\underset{\sim}{E}^1 = (\underset{\sim}{v}+\underset{\sim}{w})\theta \tag{39}$$

where θ is a small positive real number, $\underset{\sim}{v}$ is a right eigenvector of $\underset{\sim}{G}\underset{\sim}{J}$ belonging to $\hat{\lambda}$, $\underset{\sim}{u}$ is the corresponding left eigenvector, and $\underset{\sim}{w}$ is orthogonal to $\underset{\sim}{v}$.[12] The arbitrariness of phase of eigenvectors gives the correct arbitrariness of phase of $\underset{\sim}{E}^1$, and θ will be fixed once the length of $\underset{\sim}{v}$ has been chosen. It is convenient to take $|\underset{\sim}{v}| = 1$ and we shall do so, though it is not strictly necessary.

Substituting the trial expression for $\underset{\sim}{E}^1$ into (36) and dividing by θ gives

$$(\underset{\sim}{G}(i\omega)\underset{\sim}{J}+\underset{\sim}{1})(\underset{\sim}{v}+\underset{\sim}{w}) = -\underset{\sim}{G}(i\omega)\theta^2\underset{\sim}{p}(\omega,\underset{\sim}{v}+\underset{\sim}{w}) + O(\theta^3) \tag{40}$$

Now $\underset{\sim}{G}(i\omega)\underset{\sim}{J} + \underset{\sim}{1}$ is not invertible at bifurcation, but condition (ii) of Theorem 3 assures us that only one eigenvalue vanishes so the matrix has rank m-1; this means its restriction to a subspace orthogonal to $\underset{\sim}{v}$ must be invertible, and the inverse will be O(1). Thus (by a suppressed implicit function argument) we can solve for $\underset{\sim}{w}$ as a function of $\underset{\sim}{v}$ and θ, and $\underset{\sim}{w}$ will be $O(\theta^2)$ and so can be removed from $\underset{\sim}{p}$ and absorbed into the $O(\theta^3)$ terms.

Premultiplying the equation by $\underset{\sim}{u}^T$ gives

$$(\hat{\lambda}(i\omega)+1)(\underset{\sim}{u}^T\underset{\sim}{v}+\underset{\sim}{u}^T\underset{\sim}{w}) = -\theta^2\underset{\sim}{u}^T\underset{\sim}{G}(i\omega)\underset{\sim}{p}(\omega,\underset{\sim}{v}) + O(\theta^3) \tag{41}$$

and we notice that $\underset{\sim}{u}^T\underset{\sim}{v}$ is O(1) (because $\hat{\lambda}(i\omega)$ is not a multiple eigenvalue) but $\underset{\sim}{u}^T\underset{\sim}{w}$ is $O(\theta^2)$. We can therefore neglect $\underset{\sim}{u}^T\underset{\sim}{w}$ too, giving

$$\hat{\lambda}(i\omega) + 1 = -\theta^2\underset{\sim}{u}^T\underset{\sim}{G}(i\omega)\underset{\sim}{p}(\omega,\underset{\sim}{v})/\underset{\sim}{u}^T\underset{\sim}{v} + O(\theta^3) = \theta^2\zeta(\omega) + O(\theta^3) \tag{42}$$

This has the required graphical interpretation (Fig. 4), namely, that $\theta^2\zeta$ is the vector joining $\hat{\lambda}$ to -1 if we neglect $O(\theta^3)$ terms; Lemma 3.1 guarantees that (42) is solved adequately even if we evaluate ζ at ω_R instead of $\hat{\omega}$, provided $|\omega_R-\hat{\omega}|$ is not too large. The formula for ζ is summarized in Table 2 for convenience in use. ∎

Lemma 3.3. (Justification of neglect of higher harmonics)

There exist $\theta_o > 0$, $\omega_o > 0$ such that if $\hat{\theta} \leq \theta_o$ and $|\hat{\omega}-\omega_R| < \omega_o$, S has a periodic solution

---

[12] A vector $\underset{\sim}{x}$ is called a right eigenvector of a matrix $\underset{\sim}{A}$ belonging to the eigenvalue λ if $\underset{\sim}{A}\underset{\sim}{x} = \lambda\underset{\sim}{x}$, and a left eigenvector if $\underset{\sim}{x}^T\underset{\sim}{A} = \lambda\underset{\sim}{x}^T$. The symbols $\underset{\sim}{u}$ and $\underset{\sim}{v}$ here are unrelated to those of Fig. 3.

$$\underset{\sim}{e}(t) = \hat{\underset{\sim}{e}} + \sum_{k=-2}^{2} \underset{\sim}{E}^k \exp ik\omega t + O(\hat{\theta}^3) \tag{43}$$

where $\omega = \hat{\omega} + O(\hat{\theta}^4)$, and $\underset{\sim}{E}^k$ are found as in Lemma 3.2. The limit cycle is unique in a neighborhood of $\hat{\underset{\sim}{e}}$ of size O(1).

Proof. Every limit cycle must have the form

$$\underset{\sim}{e}(t) = \hat{\underset{\sim}{e}} + \underset{\sim}{e}_o(t) + \underset{\sim}{e}^*(t) \tag{44}$$

where $\underset{\sim}{e}_o = \sum_{k=-2}^{2} \underset{\sim}{E}^k \exp ik\omega t$ and $\underset{\sim}{e}^* \in P^*$, the subspace orthogonal to $\exp ik\omega t$ (k=0,1,2) on the Hilbert space P of periodic functions of period $2\pi/\omega$. (Thus $\underset{\sim}{e}^*$ consists of third and higher harmonics.)

Allwright shows [14] that for small enough $|\underset{\sim}{e}_o|$, $\underset{\sim}{e}^*$ is defined as a unique C^1 function of $\underset{\sim}{e}_o$ by the component of (44) in P^*; the $\underset{\sim}{e}^*$ so obtained is $O(|\underset{\sim}{e}_o|^3)$. The technique uses the contraction mapping theorem as in [23] and condition (ii) is again needed to ensure there is no resonance at multiples of the bifurcation frequency.

Looking at components orthogonal to P^* we must satisfy

$$\underset{\sim}{E}^k = -\underset{\sim}{G}(ik\omega)\underset{\sim}{F}^k(\underset{\sim}{e}_o, \underset{\sim}{e}^*(\underset{\sim}{e}_o)) \tag{45}$$

where $\underset{\sim}{e}_o = \sum_{k=-2}^{2} \underset{\sim}{E}^k \exp ik\omega t$. Thus

$$\underset{\sim}{E}^k = -\underset{\sim}{G}(ik\omega)\underset{\sim}{F}^k(\underset{\sim}{E}^0, \underset{\sim}{E}^1, \underset{\sim}{E}^2) + O(|\underset{\sim}{e}_o|^4) \tag{46}$$

is to be solved for $\underset{\sim}{E}^k$ (k=0,1,2) and ω. But this is precisely the problem solved in Lemma 3.2, since the $O(|\underset{\sim}{e}_o|^4)$ terms may be absorbed into the $O(|\underset{\sim}{E}^1|^4)$ terms from (33) onwards. (Note that $|\underset{\sim}{e}^*|$ is $O(|\underset{\sim}{e}_o|^3)$ but the effect on $\underset{\sim}{F}^k$ ($|k| \leq 2$) is $O(|\underset{\sim}{e}_o|^4)$ because the fact that $\underset{\sim}{e}^*$ contains only higher harmonics means it can only affect, say $\underset{\sim}{E}^2$ through terms like $\underset{\sim}{E}^1\underset{\sim}{E}^3$.) Thus by Lemmas 3.1 and 3.2, the intersection corresponds, if $\hat{\theta}$ and $|\hat{\omega}-\omega_R|$ are small enough, to a unique second order harmonic balance solution which is close to an essentially unique Fourier expansion of a periodic solution.

Proof of Theorem 3.

Lemmas 3.1, 3.2, and 3.3 prove part (a).

For part (b), note that condition (ii) ensures that the number of encirclements of -1 by branches other than $\hat{\lambda}$ is the same as the number of encirclements of $\hat{P} + \zeta\delta$ by those branches. Consequently, results of [15] ensure that there are precisely two poles of $\underset{\sim}{H}(s)$ which do not have real part negative. (This is

the only place where we make use of finite dimensionality since the fact that S is equivalent to $\mathcal{D}$ is used in all the published proofs of the characteristic locus method. But see [21].)

Allwright shows [14] that one of these two is zero and the other has sign determined by ζ in the required way. The method is to use Mees's technique for determining the characteristic exponents from the harmonic balance solution [29]. More restrictions on the size of θ may be required, which is why θ_1 and ω_1 appear in the statement of (b). ¤

3.3. Algebraic versions of the graphical results

The graphical Hopf theorem gives us values for ω, $\underset{\sim}{E}^0$, $\underset{\sim}{E}^1$, and $\underset{\sim}{E}^2$ that are accurate to second order in θ. Several authors [6,13,14,10] have given equivalent algebraic formulae in terms of a first approximation and a second order correction. To facilitate comparison with their results, and because it is sometimes useful to have the formulae available, we now show how to derive expressions for the "curvature coefficient" σ_o of Sec. 2 and the difference $\delta\omega$ between $\hat{\omega}$, the imaginary part of the bifurcating eigenvalue, and ω, the Hopf approximation to the oscillation frequency.

Suppose s is such that $\underset{\sim}{G}(s)\underset{\sim}{J}$ has an eigenvalue which is -1; clearly, $\underset{\sim}{G}(\bar{s})\underset{\sim}{J}$ will also have such an eigenvalue, and if $\mu = \mu_o$ (i.e., exactly at bifurcation) then $s = i\omega_o$, $\bar{s} = -i\omega_o$. As μ increases beyond μ_o, s moves into the right half of the complex plane, taking the value $\alpha + i\omega$, say, with $\alpha > 0$, $\omega > 0$.[13] Let us assume μ is fixed at some value beyond μ_o for which the techniques of Sec. 3.2 ensure a solution.

We want to estimate the value of $\hat{\omega}$ satisfying (36) in terms of α and ω. If $\underset{\sim}{v}$ and $\underset{\sim}{u}$ are now written for the right and left eigenvectors of $\underset{\sim}{G}(s)\underset{\sim}{J}$ corresponding to the eigenvalue -1, we can try the solution

$$\underset{\sim}{E}^1 = (\underset{\sim}{v}+\underset{\sim}{w})\theta \tag{47}$$

in (36), where $\underset{\sim}{w}$ is orthogonal to $\underset{\sim}{v}$. Now write

$$\underset{\sim}{G}(i\hat{\omega}) = \underset{\sim}{G}(s) + (-\alpha+i\delta\omega)\underset{\sim}{G}'(s) + O(|s-i\hat{\omega}|^2)$$

where $\delta\omega \triangleq \omega - \hat{\omega}$ and $\underset{\sim}{G}'$ is the derivative of $\underset{\sim}{G}$ with respect to s, evaluated at our given s. Using this and (47) in (36) we have

[13] Note that s and $\bar{s}$ are just the "bifurcating eigenvalues," i.e., the local continuation of the eigenvalues of the linearized state space equations for values of μ greater than μ_o.

$$\underset{\sim}{u}^T\left\{\left[\underset{\sim}{G}(s)-\underset{\sim}{G}'(s)(\alpha-i\delta\omega)\underset{\sim}{J}+\underset{\sim}{1}\right\}(\underset{\sim}{v}+\underset{\sim}{w}) = -\theta^2\underset{\sim}{u}^T\underset{\sim}{G}(i\hat{\omega})\underset{\sim}{p}(\hat{\omega},\underset{\sim}{v}+\underset{\sim}{w}) + O(\theta^3) + O(|s-i\hat{\omega}|^2)\right. \tag{48}$$

Because $\underset{\sim}{u}$ is a left eigenvector of $\underset{\sim}{G}(s)\underset{\sim}{J}$ we can rewrite (48) as

$$-\underset{\sim}{u}^T\underset{\sim}{G}'(s)(\alpha-i\delta\omega)\underset{\sim}{J}\underset{\sim}{v} = -\underset{\sim}{u}^T\underset{\sim}{G}(i\hat{\omega})\underset{\sim}{p}(\hat{\omega},\underset{\sim}{v})\theta^2 + O(\theta^3) + O(|s-i\hat{\omega}|^2) \tag{49}$$

where we have absorbed $\underset{\sim}{w}$ into the $O(\theta^3)$ terms as in Lemma 3.2.

Now for fixed θ, we can use an implicit function argument to show that s and $i\hat{\omega}$ are both within $O(\theta^2)$ of $i\omega$, so we can rewrite (49) as follows:

$$\alpha - i\delta\omega = \left\{\frac{\underset{\sim}{u}^T\underset{\sim}{G}(i\omega)\underset{\sim}{p}(\omega,\underset{\sim}{v})}{\underset{\sim}{u}^T\underset{\sim}{G}'(i\omega)\underset{\sim}{J}\underset{\sim}{v}}\right\}\theta^2 + O(\theta^3) \tag{50}$$

Call the right side of (50) $\nu\theta^2 + O(\theta^3)$. First we take the real part of (50). To have a solution for small $\theta^2 > 0$ we need α and Re ν to have the same sign, or $\alpha\sigma_o < 0$ where $\sigma_o = -\text{Re }\nu$; i.e.,

$$\boxed{\sigma_o = -\text{Re}\left\{\frac{\underset{\sim}{u}^T\underset{\sim}{G}(i\omega)\underset{\sim}{p}(\omega,\underset{\sim}{v})}{\underset{\sim}{u}^T\underset{\sim}{G}'(i\omega)\underset{\sim}{J}\underset{\sim}{v}}\right\}} \tag{51}$$

This is the formula referred to in Sec. 2, Theorem 2, and is the result obtained by Allwright [14] who shows it reduces to Poore's formula [13] in the special case of an ordinary differential equation. It is straightforward but tedious to show that if one writes a second order O. D. E. in the form of (1) and calculates σ_o from (51), the result is identical to that given by (14). Notice the two advantages of using (51) rather than Marsden and McCracken's result for σ_o: there is no coordinate change to make and the size of the matrices in (51) is never greater than the dimension of the state space representation, and is often very much less.

Now if we take the imaginary part of (50) we have

$$\delta\omega = -\theta^2\text{Im }\nu = -\frac{\alpha\text{Im }\nu}{\text{Re }\nu} \tag{52}$$

and the limit cycle has frequency $\omega + \delta\omega + O(\theta^4)$ or, using $\alpha = O(\theta^2)$, the frequency is

$$\boxed{\hat{\omega} = \omega - \frac{\alpha\text{Im }\nu}{\text{Re }\nu} + O(\alpha^2)} \tag{53}$$

which is just the frequency $\hat{\omega}$ read off by the graphical method.

4. Examples of Applications of the Hopf Bifurcation Theorem

To illustrate how to apply the Hopf theorem in practice, we present three examples in this final section. Both the time-domain (Theorem 2) and the frequency-domain (Theorem 3) version of the theorem are illustrated in Example 1 to show that

they indeed give the same answers. However, only Theorem 3 is applied in Examples 2 and 3 since to use Theorem 2 would have involved a great deal more work. This observation thus confirms our earlier assertion that the graphical approach of Theorem 3 would be the most widely used in practice.

Example 1.

Consider the single tunnel-diode oscillator circuit shown in Fig. 5(a) with the typical I_D-V_D curve for the tunnel diode shown in Fig. 5(b). The state equations are easily found to be:

$$\dot{i}_L = (1/L)v_C \tag{54a}$$

$$\dot{v}_C = (1/C)\left[g(V_B - v_C) - i_L\right] \tag{54b}$$

Let us assume that $g(\cdot)$ is a C^4-function and that $g'(\mu_o) = 0$, $g''(\mu_o) < 0$, and $g'''(\mu_o) > 0$. Replacing (i_L, v_C) by (x_1, x_2) and choosing $L = C = 1$ to simplify calculation makes (54) assume the form:

$$\dot{x}_1 = x_2 \triangleq f_1(x_1, x_2; \mu) \tag{55a}$$

$$\dot{x}_2 = g(\mu - x_2) - x_1 \triangleq f_2(x_1, x_2; \mu) \tag{55b}$$

where the bias voltage V_B is chosen as the parameter μ. The equilibrium point is located at $\hat{x}_1 = g(\mu)$ and $\hat{x}_2 = 0$. The two complex-conjugate eigenvalues of the associated Jacobian matrix evaluated at $(\hat{x}_1, \hat{x}_2)$ are:

$$\lambda_{1,2} = -\frac{1}{2} g'(\mu) \pm i \sqrt{1 - \left[\frac{1}{2} g'(\mu)\right]^2} \triangleq \alpha(\mu) \pm i\omega(\mu) \tag{56}$$

The loci of λ_1 and λ_2 are sketched in Fig. 5(c) for $\mu_1 \leq \mu \leq \mu_2$. Observe that since $g'(\mu_o) = 0$ and $g''(\mu_o) < 0$, we have $\alpha(\mu_o) = 0$, $\omega(\mu_o) = 1$, and $\alpha'(\mu_o) > 0$. Since the Jacobian

$$\underset{\sim}{J}(\mu_o) = \begin{bmatrix} 0 & 1 \\ -1 & -g'(\mu_o) \end{bmatrix} = \begin{bmatrix} 0 & 1 \\ -1 & 0 \end{bmatrix} \tag{57}$$

at $\mu = \mu_o$ is already in the standard form (2c), we have $\underset{\sim}{f}(x;\mu) = \underset{\sim}{\tilde{f}}(x;\mu)$. Hence we can apply Theorem 2 directly, without having to change coordinates. In this case, criticality occurs at $\mu = \mu_o$ and the bifurcation frequency is $\omega_o = 1$. Since all partial derivatives (up to 3rd order) vanish except $\tilde{f}^2_{22} = g''(\mu_o)$ and $\tilde{f}^2_{222} = -g'''(\mu_o)$, the curvature coefficient in (14) is simply given by $\sigma_o = -\frac{1}{4} g'''(\mu_o) < 0$. It follows from Theorem 2 that there exists an $\varepsilon > 0$ such that (55) has a stable limit cycle for all $\mu_o \leq \mu < \mu_o + \varepsilon$.

Observe that since $\alpha(\mu)$ also vanishes at $\mu = \mu_o'$ in Fig. 5(b), we can define another parameter $\nu = -\mu$ and replace (55b) by $g(\mu - x_2) = g(-\nu - x_2)$, so that the associated eigenvalue will again cross the $j\omega$-axis from left to right as ν increases. Using the same analysis as before, we conclude that there exists an $\varepsilon > 0$ such that (55) has a stable limit cycle for all $\mu_o' - \varepsilon < \mu \leq \mu_o'$.

Let us analyze next the same circuit using Theorem 3. Our first task is to transform (55) into an equivalent feedback system as in Fig. 5(d). One simple choice is $G(s) = \frac{s}{s^2+1}$ and $f(e) = -g(\mu - e)$. In this case, however, $\hat{\lambda}(i\omega) = G(i\omega)J(\mu_o)$ is purely imaginary. There is no conceptual or theoretical difficulty here since we can always use the Riemann sphere to draw the conclusion that bifurcation will take place at the north pole (i.e., at ∞ in the complex plane). However, this is a nuisance in practice and since (17) allows us to find infinitely many other equivalent systems, let us simply choose a more convenient representation. One such choice is:

$$\underset{\sim}{A} = \begin{bmatrix} 0 & 1 \\ -1 & 0 \end{bmatrix}, \quad \underset{\sim}{B} = \begin{bmatrix} 0 \\ -1 \end{bmatrix}, \quad \underset{\sim}{C} = [0 \ -1], \quad \underset{\sim}{D} = [-1], \quad g(y;\mu) \triangleq -g(\mu+y) \tag{58}$$

Substituting (58) into (19), we obtain:

$$G(s) = \frac{s}{s^2+s+1}, \quad f(e;\mu) = -g(\mu - e) - e \tag{59}$$

To apply the graphical Hopf theorem, we first solve $G(0)f(e;\mu) + e = 0$ to obtain the equilibrium point $\hat{e} = 0$. Next we sketch[14] the eigenvalue locus $\hat{\lambda}(i\omega)$ of $\underset{\sim}{G}(i\omega)\underset{\sim}{J}$ and compute $\zeta(\omega_R)$ from Table 2:

Step 1. $G(i\omega) = \frac{i\omega}{(1-\omega^2)+i\omega}$, $J(\mu) = f'(0;\mu) = g'(\mu) - 1$

$$\therefore \quad \hat{\lambda}(i\omega) = G(i\omega)\, J(\mu) = \left[g'(\mu)-1\right] \left[\frac{\omega^2 + i\omega(1-\omega^2)}{(1-\omega^2)^2 + \omega^2}\right]$$

Since $\operatorname{Im} \hat{\lambda}(i\omega) = 0$ when $\omega = 1$, we identify $\omega_R = 1$. Moreover, since $\hat{\lambda}(i\omega) = -1$ when $\omega = 1$ and $\mu = \mu_o$, we have $\omega_o = \omega_R$ and criticality occurs at $\mu = \mu_o$. Since $G(i\omega)\, J(\mu)$ is a scalar, the right and left eigenvectors are given trivially by $v = 1$ and $u = 1$.

Step 2. Q is a scalar in this case:

$$Q = f''(\mu_o) = -g''(\mu_o) > 0$$

[14] We only need to plot $\hat{\lambda}(i\omega)$ accurately in the neighborhood of $\omega = \omega_R$ to ensure an accurate intersection point $\hat{P}$.

Step 3. $H(0) = \left[G(0)J(\mu_o)+1\right]^{-1} G(0) = 0$

$$H(i2) = \left[G(i2)\ J(\mu_o) + 1\right]^{-1} G(i2) = (-i2)/3$$

$$\therefore\ v^0 = -\frac{1}{4} H(0)\, Q\bar{v} = 0$$

$$v^2 = -\frac{1}{4} H(i2)\ Qv = -\frac{i}{6} g''(\mu_o)$$

Step 4. $L = f'''(\mu_o)(1)(1) = g'''(\mu_o)$

$$p(\omega_R, v) = Q\, v^0 + \frac{1}{2}\bar{Q}v^2 + \frac{1}{8} L\bar{v} = \frac{1}{8} g'''(\mu_o) + \frac{i}{12}\left[g''(\mu_o)\right]^2$$

Step 5. $$\zeta(\omega_R) = \frac{-uG(i1)p(\omega_R, v)}{uv} = -\frac{1}{8} g'''(\mu_o) - \frac{i}{12}\left[g''(\mu_o)\right]^2 \qquad (60)$$

Observe that since $g'''(\mu_o) > 0$ and $\left[g''(\mu_o)\right]^2 > 0$, the vector from the point $-1 + i0$ in the direction $\zeta(\omega_R)$ is located in the 3rd quadrant (relative to -1) as shown in Fig. 5(e). Since the locus of $\hat{\lambda}(i\omega)$ passes through -1 when $\mu = \mu_o$; we have $\hat{\theta} = 0$ and it follows from Theorem 3 that when $V_B = \mu_o$, the circuit of Fig. 5(a) has a stable limit cycle of zero amplitude.

The locus of $\hat{\lambda}(i\omega)$ corresponding to different values of μ is shown in Figs. 5(f) to 5(j), along with the vector from -1 in the direction $\zeta(\omega_R)$. Observe that as μ increases, the locus expands, intersects the vector, and then shrinks again. It follows from Theorem 3 that no limit cycle exists when $\mu < \mu_o$ and when $\mu > \mu_o'$, while a locally stable limit cycle exists for $\mu_o \leq \mu < \mu_o + \varepsilon$, and for $\mu_o' - \varepsilon < \mu \leq \mu_o'$. These conclusions are completely consistent with those predicted earlier using the time-domain Hopf theorem, as they should be.

Example 2.

The well-known Wien bridge oscillator circuit [4] is shown in Fig. 6(a). The operational amplifier (OP AMP) and the two resistors R_S and R_F can be modeled by a nonlinear voltage-controlled voltage source $F(v_{C_2})$ as shown in Fig. 6(b). The function $F(v_{C_2})$ can be approximated by the piecewise-linear function shown in Fig. 6(c). The state equations for this circuit are easily found to be given by:

$$\dot{v}_{C_1} = -\frac{1}{RC_1}\left[v_{C_1} + v_{C_2} - F(v_{C_2})\right] \qquad (61a)$$

$$\dot{v}_{C_2} = -\frac{1}{RC_2}\left[v_{C_1} + 2v_{C_2} - F(v_{C_2})\right] \qquad (61b)$$

If we let $x_1 = v_{C_1}$, $x_2 = v_{C_2}$, $k_1 = 1/RC_1$ and $k_2 = 1/RC_2$, then (61) assumes the form

$$\dot{x}_1 = -k_1(x_1+x_2) + k_1 F(x_2) \tag{62a}$$

$$\dot{x}_2 = -k_2(x_1+2x_2) + k_2 F(x_2) \tag{62b}$$

Equation (62) has an equilibrium point at $\hat{x}_1 = 0$, $\hat{x}_2 = 0$. Chua and Green [24] have recently proved that this equilibrium point is a global attractor if $|F(x_2)/x_2| < 2$ for all $x_2 \neq 0$. To turn this circuit into an oscillator, a general design guideline [4] is to choose R_S and R_F such that $A \triangleq (R_S+R_F)/R_S \geq 3$, where "A" is the slope of the linear segment at the origin in Fig. 6(c). This guideline was derived by a linearized analysis where it can be shown that a pair of complex-conjugate eigenvalues crosses the $j\omega$-axis at $i\omega_o$ into the RHP when A increases beyond 3. It is observed experimentally that the circuit oscillates with a nearly sinusoidal waveform at frequency ω_o if $A = 3+\varepsilon$, where ε is a sufficiently small number. For large ε, the waveform is found to be highly distorted and the frequency is observed to depart significantly from ω_o. In spite of its widespread usage, no rigorous theoretical analysis of the Wien bridge oscillator has appeared in the literature because such an analysis must necessarily be nonlinear and very few tools are available for predicting the existence of an oscillation, let alone an estimate of its amplitude and frequency. We will now show that the Hopf theorem fills this need admirably.

Without loss of generality, assume $k_1 = k_2 = 1$. An inspection of (62) shows that the Jacobian matrix evaluated at $\hat{x} = 0$ is <u>not</u> in the standard form as specified by (2c). Hence, a change of coordinates will be necessary before Theorem 2 can be applied. Moreover, there is no natural parameter μ available from (62).[15] However, both difficulties disappear if we choose to use the graphical Hopf theorem instead. As before, our first step is to find a suitable equivalent feedback representation of (62) as shown in Fig. 6(d). Although $G(s)$ can be made into a scalar by a suitable choice of A, B, C, and D in (17), we will choose instead

[15] On hindsight, it is clear that A is a suitable parameter. However, this is far from obvious before one makes a linearized analysis of (62).

$$\underset{\sim}{A} = \begin{bmatrix} -1 & -1 \\ -1 & -2 \end{bmatrix}, \quad \underset{\sim}{B} = \begin{bmatrix} 1 & 0 \\ 0 & 1 \end{bmatrix}, \quad \underset{\sim}{C} = [0 \ -1], \quad \underset{\sim}{D} = \begin{bmatrix} 0 \\ 0 \end{bmatrix}, \quad \underset{\sim}{g}(y;\mu) \triangleq \begin{bmatrix} F(-y) \\ F(-y) \end{bmatrix} \tag{63}$$

in order to emphasize that $\underset{\sim}{G}$ need not be a square matrix; namely,

$$\underset{\sim}{G}(s) = \underset{\sim}{C}(\underset{\sim}{A}-s\underset{\sim}{1})^{-1}\underset{\sim}{B} = \begin{bmatrix} \frac{1}{s^2+3s+1} & \frac{-(s+1)}{s^2+3s+1} \end{bmatrix} \tag{64a}$$

$$\underset{\sim}{f}(e) = \begin{bmatrix} F(e) \\ F(e) \end{bmatrix} \tag{64b}$$

Similarly, even though the parameter μ need not be explicitly specified, we will choose $A = \mu$ in order to compare our results with heuristic design guidelines. In order to apply the Hopf theorem, we must first replace the piecewise-linear functions $F(v_{C_2})$ in Fig. 6(c) by a C^3-function whose 2nd and 3rd order derivatives do not all vanish at the equilibrium point $\hat{e} = 0$. A reasonable approximation for $F(e)$ is given by:

$$F(e) = \frac{2}{\pi} E \arctan\left(\frac{\pi}{2}\frac{A}{E} e\right) \tag{65}$$

where $F(e) \to \pm E$ as $e \to \pm\infty$, and where $F'(0) = A$, as shown in Fig. 6(e). If we choose $\mu = A$, then

$$\underset{\sim}{G}(s)\ \underset{\sim}{J}(\mu) = \begin{bmatrix} \frac{1}{s^2+3s+1} & \frac{-(s+1)}{s^2+3s+1} \end{bmatrix}\begin{bmatrix} \mu \\ \mu \end{bmatrix} = \frac{-\mu s}{s^2+3s+1} \tag{66}$$

We are now ready to compute the various quantities in Table 2:

Step 1.

Sketch the eigenvalue locus $\hat{\lambda}(i\omega)$ of $\underset{\sim}{G}(i\omega)\underset{\sim}{J}$ at the equilibrium point $\hat{e} = 0$:

$$\hat{\lambda}(i\omega) = \underset{\sim}{G}(i\omega)\ \underset{\sim}{J}(\mu) = \frac{-3\omega^2\mu - i\mu\omega(1-\omega^2)}{(1-\omega^2)^2 + (3\omega)^2} \tag{67}$$

When $\omega = 1$, Re $\hat{\lambda}(i\omega) = -\mu/3$ and Im $\hat{\lambda}(i\omega) = 0$. Thus $\omega_R = 1$ and criticality occurs at $\mu = 3$. Since $\underset{\sim}{G}(i\omega)\ \underset{\sim}{J}(\mu)$ is a scalar, $v = 1$ and $u = 1$.

Step 2. $Q = \begin{bmatrix} F''(0) \\ F''(0) \end{bmatrix} = \begin{bmatrix} 0 \\ 0 \end{bmatrix}$

Step 3. $v^0 = 0, \quad v^2 = 0$

Step 4. $\underset{\sim}{L} = \begin{bmatrix} F'''(0) \\ F'''(0) \end{bmatrix}$, where $F'''(0) = \frac{-\pi^2}{2E^2}\mu^3$

$$\underset{\sim}{p}(\omega_R, v) = \underset{\sim}{Q}\underset{\sim}{v}^0 + \frac{1}{2}\underset{\sim}{\bar{Q}}\underset{\sim}{v}^2 + \frac{1}{8}\underset{\sim}{L}\bar{v} = \begin{bmatrix} \frac{-\pi^2}{16E^2}\mu^3 \\ \frac{-\pi^2}{16E^2}\mu^3 \end{bmatrix}$$

$$\text{Step 5.} \quad \zeta(\omega_R) = \frac{-\underset{\sim}{u}^T \underset{\sim}{G}(i\omega_R)\underset{\sim}{p}(\omega_R, \underset{\sim}{v})}{\underset{\sim}{u}^T\underset{\sim}{v}} = -\frac{\pi^2}{48E^2}\mu^3 \tag{68}$$

Observe that $\zeta(\omega_R)$ is a negative real number for any μ. Hence the vector from -1 in the direction $\zeta(\omega_R)$ is simply a horizontal vector pointing towards the left, as shown in Figs. 6(f), (g), and (h) for 3 different values of $\mu \triangleq A$. It follows from the graphical Hopf theorem that the circuit in Fig. 6(a) has a locally stable nearly sinusoidal oscillation when $A = 3(1+\epsilon)$ where ϵ is a sufficiently small number.

Example 3.

Our final example is taken not from circuit theory but from mathematical biology, but we believe it shows the power of the graphical approach (Theorem 3) particularly well. Mees and Rapp [8] considered a model of a metabolic oscillator which led to the equations

$$\left.\begin{aligned} \dot{x}_1 &= \frac{1}{1+x_n} - b_1 x_1 \\ \dot{x}_2 &= \frac{x_1}{1+x_n} - b_2 x_2 \\ \dot{x}_j &= x_{j-1} - b_j x_j, \quad 3 \le j \le n \end{aligned}\right\} \tag{69}$$

where $n \ge 3$ and $b_j > 0$ for all j. Since the x_j represent concentrations, we are interested in the positive orthant $x_j \ge 0$. There is exactly one equilibrium point in the positive orthant and it is known to be a global attractor if all the b_j are large enough [8].

As the b_j decrease, the equilibrium point ceases to be locally attracting; the easiest way to see this is to transform (69) into the equivalent feedback form in Fig. 7(a), where

$$\underset{\sim}{G}(s;\mu) = \begin{bmatrix} \dfrac{1}{(s+b_1)} & 0 \\ 0 & \dfrac{1}{(s+b_2)(s+b_3)\cdots(s+b_n)} \end{bmatrix} \tag{70a}$$

$$\underset{\sim}{f}(\underset{\sim}{e}) = \begin{bmatrix} f_1(\underset{\sim}{e}) \\ f_2(\underset{\sim}{e}) \end{bmatrix} = \begin{bmatrix} \dfrac{-1}{1+e_2} \\ \dfrac{-e_1}{1+e_2} \end{bmatrix} \tag{70b}$$

Equation (70) is obtained from (69) and (19) with the following choices:

$$\underset{\sim}{A} = \begin{bmatrix} -b_1 & 0 & 0 & 0 & 0 \cdots 0 & 0 \\ 0 & -b_2 & 0 & 0 & 0 \cdots 0 & 0 \\ 0 & 1 & -b_3 & 0 & 0 \cdots 0 & 0 \\ 0 & 0 & 1 & -b_4 & 0 \cdots 0 & 0 \\ \vdots & \vdots & \vdots & \vdots & \vdots \quad \vdots & \vdots \\ 0 & 0 & 0 & 0 & 0 \cdots 1 & -b_n \end{bmatrix}, \quad \underset{\sim}{B} = \begin{bmatrix} -1 & 0 \\ 0 & -1 \\ 0 & 0 \\ 0 & 0 \\ \vdots & \vdots \\ 0 & 0 \end{bmatrix}, \quad \underset{\sim}{D} = \begin{bmatrix} 0 & 0 \\ 0 & 0 \end{bmatrix}$$

and $\underset{\sim}{C} = \begin{bmatrix} -1 & 0 & 0 & 0 \cdots 0 & 0 \\ 0 & 0 & 0 & 0 \cdots 0 & -1 \end{bmatrix}$, and $\underset{\sim}{g}(y;\mu) = \begin{bmatrix} \dfrac{-1}{1-y_2} \\ \dfrac{y_1}{1-y_2} \end{bmatrix}$

The equilibrium point $\hat{\underset{\sim}{e}} = (\hat{e}_1, \hat{e}_2)$ is obtained by solving (20); namely,

$$\hat{e}_1 = \frac{1}{b_1(1+\hat{e}_2)} \tag{71a}$$

$$\hat{e}_2(1+\hat{e}_2)^2 = \frac{1}{b_1 b_2 \cdots b_n} \, . \tag{71b}$$

Nyquist's criterion can be used to study the local stability and it can be shown [8] that there is only one candidate for a stable limit cycle; namely, the first limit cycle to bifurcate from the equilibrium point as $c \triangleq b_1 b_2 \cdots b_n$ decreases. If "n" is large, the formulas for σ_o for the time-domain Hopf theorem as given by Marsden and McCracken [10] and others are difficult to apply. The enormous computational advantages of the frequency-domain approach allow us to say a good

deal more about the system than was possible in [8]. Indeed, $\underset{\sim}{G}(s)\,\underset{\sim}{J}(\mu)$ is only a 2x2 matrix (independent of "n"!) with just two eigenvalues. The condition $\hat{\lambda}(i\omega) = -1$ determines ω_o as a function of $b = [b_1, b_2, \ldots, b_n]^T$ and restricts b at bifurcation to lie on a manifold of codimension 1 in $\mathbb{R}^n_+$. We can consider bifurcation along any curve $\underset{\sim}{b}(\mu)$ which intersects this manifold transversally: in many cases, Theorem 3 frees us from the need to specify $\underset{\sim}{b}(\mu)$ explicitly.

We could go further analytically and show that for sufficiently large n, the limit cycle is certainly stable just after bifurcation, but for present purposes it is probably more interesting to take a numerical example. Figure 7(b) shows the $\hat{\lambda}(i\omega)$ loci when n = 15 and $b_j = b = 0.799$ for all j, confirming the statement in [8] that this is the first bifurcation present for n = 15 and for identical b_j values. The vector from the point -1 in the direction $\zeta(\omega_R)$ is shown intersecting $\hat{\lambda}(i\omega)$ at the point -1 and pointing outward. Hence, it follows from Theorem 3 that there exists a stable limit cycle (of zero amplitude) with an angular frequency $\omega = 0.176$.

As b decreases, the loci expand and $|\zeta(\omega_R)|$ decreases: when b = 0.7, we obtain Fig. 7(c), where $\hat{\omega} = 0.170$ and $|\zeta(\omega_R)| \cong 2\text{x}10^{-2}$, $\hat{\theta} \approx 3$ so already we may not be able to neglect $O(\theta^3)$ and our theorem seems unlikely to make useful quantitative predictions. If we neglect this and look at the case b = 0.1 as shown in Fig. 7(d), we find $|\zeta(\omega_R)| \cong 10^{-10}$, $\hat{\theta} \cong 6\text{x}10^4$ and in fact the predicted angular frequency is $\hat{\omega} = 0.025$ and the predicted peak value of e is $1.8\text{x}10^5$. This case was simulated by Mees and Rapp [8] who found values of 0.019 and $9\text{x}10^6$, respectively. So the frequency is surprisingly good but the amplitude prediction is useless.

The point of all this is that the Hopf theorem only makes predictions for an unspecified, probably small range of $\hat{\theta}$ values but experience tends to confirm that predictions often remain <u>qualitatively</u> correct even when the system is very far from bifurcation. This is not surprising if one imagines how the limit cycle grows out from equilibrium in the state space: even if the limit cycle itself bifurcates repeatedly, there will always be at least one limit cycle present (not necessarily stable). If it does not grow to infinite amplitude it can only disappear completely either by collapsing back into the equilibrium, as in Example 1 when $\mu \to \mu_o'$, or by coalescing with another limit cycle having complementary stability properties: this other limit cycle would have to have been generated by an independent bifurcation process.

Acknowledgments

The authors would like to thank Peter Swinnerton-Dyer, David Allwright and Paul Rapp for many useful comments and discussions.

REFERENCES

1. K. K. Clarke and D. T. Hess, Communication Circuits: Analysis and Design, Addison-Wesley Publishing Company, Reading, Mass., 1971.
2. H. J. Reich, Functional Circuits and Oscillators, Van Nostrand, New York, N.Y., 1961.
3. L. O. Chua and Y. W. Sing, "A nonlinear lumped circuit model for Gunn diodes," International Journal of Circuit Theory and Applications, to appear.
4. J. Millman and C. C. Halkias, Integrated Electronics: Analog and Digital Circuits and Systems, McGraw-Hill Book Company, New York, N.Y. 1972.
5. J. Kudrewicz, "Contribution to the theory of weakly nonlinear oscillators, Part I: An estimate of amplitude and frequency, and Part II, Generalized Lindstedt's method," International Journal of Circuit Theory and Applications, vol. 4. 1976, pp. 161-176.
6. J. Kudrewicz and M. Odyniec, "Periodic oscillations in autonomous systems," Archiwum Elektrotechniki, vol. XXIII, no. 2, 1974, pp. 265-276 (in polish).
7. E. Hopf, "Bifurcation of a periodic solution from a stationary solution of a system of differential equations," Berrichten der Mathematische Physikalische Klasses der Sachischen Acad. Wissenschaften, Leipzig XCIV, 1942, pp. 3-22.
8. A. I. Mees and P. E. Rapp, "Periodic metabolic systems," to appear in J. Math. Biology, 1978.
9. N. MacDonald, "Bifurcation theory applied to a simple model of a biochemical oscillator," Preprint, 1975.
10. J. Marsden and M. McCracken, The Hopf Bifurcation and its Applications, Applied Mathematical Sciences, vol. 19, Springer-Verlag, New York, N.Y. 1976.
11. D. Ruelle and R. Takens, "On the nature of turbulence," Communications in Mathematical Physics, vol. 20, 1971, vol. 20, pp. 167-192 and vol. 23, pp. 343-344.
12. N. Kopell and L. N. Howard, "Pattern formation in the Belousov reaction," in Lectures on Mathematics in the Life Series," American Mathematical Society, vol. 7, 1974, pp. 201-216.
13. A. B. Poore, "On the theory and application of the Hopf-Friedrichs bifurcation theory," Archive of Rational Mechanics and Analysis, vol. 60, 1976, pp. 371-393.
14. D. J. Allwright, "Harmonic balance and the Hopf bifurcation theorem," Math. Proc. Cambridge Philosophical Society, vol. 82, 1977, pp. 453-467.

15. A. G. J. MacFarlane and I. Postlethwaite, "The generalized Nyquist stability criterion and multivariable root loci," International Journal on Control, vol. 25, 1977, pp. 81-127.

16. P. Swinnerton Dyer, "The Hopf bifurcation theorem in three dimensions," Math. Proc. of Cambridge Philosophical Society, vol. 82, 1977, pp. 469-483.

17. H. S. Wilf, Mathematics for the Physical Sciences, John Wiley and Sons, Inc., New York, N.Y. 1962.

18. J. K. Hale, Ordinary Differential Equations, John Wiley and Sons, New York, N.Y. 1969.

19. L. O. Chua, Introduction to Nonlinear Network Theory, McGraw-Hill Book Company, New York, N.Y. 1969.

20. A. Kelley, "The stable, center-stable, center, center-unstable, and unstable manifolds," Appendix C of Transversal Mappings and Flows, by R. Abraham and J. Robbin, W. A. Benjamin, Inc., New York, N.Y. 1967, pp. 134-154.

21. Edmunds (personal communication), to be submitted to International Journal on Control.

22. A. R. Bergen and R. L. Franks, "Justification of the describing function method," SIAM J. Control, vol. 9, no. 4, Nov. 1971, pp. 568-589.

23. A. I. Mees and A. R. Bergen, "Describing functions revisited," IEEE Trans. on Automatic Control, vol. AC-20, no. 4, August 1975, pp. 473-478.

24. L. O. Chua and D. N. Green, "A qualitative analysis of the behavior of dynamic nonlinear networks: stability of autonomous networks," IEEE Trans. Circuits and Systems, vol. CAS-23, no. 6, June 1976, pp. 355-379.

25. A. I. Mees, "The describing function matrix," Journal of the Institute of Mathematics and its Applications, vol. 10, 1972, pp. 49-67.

26. D. Williamson, "Periodic motion in nonlinear systems," IEEE Trans. Automatic Control, vol. AC-20, no. 4, August 1975, pp. 479-486.

27. A. G. J. MacFarlane and I. Postlethwaite, "Extended principle of the argument," to appear in International Journal on Control, 1977.

28. R. L. Bishop and S. I. Goldberg, Tensor Analysis on Manifolds, The Macmillan Company, New York, N. Y., 1968.

29. A. I. Mees, "Limit cycle stability," Journal of Institute of Mathematical Applications, vol. 11, 1973, pp. 281-295.

Table 1. Values for Coefficients of V

Parameter in V	Value to make $\dot{V}$ sign definite
a	$-\left\{\tilde{f}^2_{22} + \tilde{f}^1_{12} + \frac{1}{2}\,\tilde{f}^2_{11}\right\}/\omega(\mu)$
b	$\frac{1}{2}\,\tilde{f}^1_{11}/\omega(\mu)$
c	$-\frac{1}{2}\,\tilde{f}^2_{22}/\omega(\mu)$
d	$\left\{\tilde{f}^1_{11} + \tilde{f}^2_{12} + \frac{1}{2}\,\tilde{f}^1_{22}\right\}/\omega(\mu)$
e	$h - \left\{\frac{1}{6}\,\omega(\mu)\,\tilde{f}^2_{111} + \frac{1}{2}\,\omega(\mu)\,\tilde{f}^1_{112} + a\tilde{f}^1_{12} + b\tilde{f}^2_{12} + b\tilde{f}^1_{11} + c\tilde{f}^2_{11}\right\}/\omega(\mu)$ $= h - \left\{\frac{1}{6}\,\omega(\mu)\,\tilde{f}^2_{111} + \frac{1}{2}\,\omega(\mu)\,\tilde{f}^1_{112} - \tilde{f}^1_{12}\tilde{f}^2_{22} - (\tilde{f}^1_{12})^2 - \frac{1}{2}\,\tilde{f}^1_{12}\tilde{f}^2_{11}\right.$ $\left. + \frac{1}{2}\,\tilde{f}^1_{11}\tilde{f}^2_{12} + \frac{1}{2}\,(\tilde{f}^1_{11})^2 + \frac{1}{2}\,\tilde{f}^2_{22}\tilde{f}^2_{11}\right\}/\omega^2(\mu)$
h	arbitrary
k	$h + \left\{\frac{1}{6}\,\tilde{f}^1_{222} + \frac{1}{2}\,\tilde{f}^2_{122} + b\tilde{f}^1_{22} + c\tilde{f}^2_{22} + c\tilde{f}^1_{12} + d\tilde{f}^2_{12}\right\}/\omega(\mu)$ $= h + \left\{\frac{1}{6}\,\omega(\mu)\,\tilde{f}^1_{222} + \frac{1}{2}\,\omega(\mu)\,\tilde{f}^2_{122} + \frac{1}{2}\,\tilde{f}^1_{11}\tilde{f}^1_{22} - \frac{1}{2}\,(\tilde{f}^2_{22})^2\right.$ $\left. - \frac{1}{2}\,\tilde{f}^2_{22}\tilde{f}^1_{12} + \tilde{f}^1_{11}\tilde{f}^2_{12} + (\tilde{f}^2_{12})^2 + \frac{1}{2}\,\tilde{f}^1_{22}\tilde{f}^2_{12}\right\}/\omega^2(\mu)$
g	must satisfy $\frac{1}{6}\,\tilde{f}^1_{111} + \frac{1}{2}\,a\tilde{f}^1_{11} + \frac{1}{2}\,b\tilde{f}^2_{11} - \omega(\mu)g < 0$, for $\dot{V} < 0$ > 0, for $\dot{V} > 0$
j	must satisfy $\frac{1}{6}\,\tilde{f}^2_{222} + \frac{1}{2}\,c\tilde{f}^1_{22} + \frac{1}{2}\,d\tilde{f}^2_{22} + \omega(\mu)j < 0$, for $\dot{V} < 0$ > 0, for $\dot{V} > 0$

Table 2. Algorithm for Computing $\zeta(\omega_R)$

Step	Algorithm
1	Given $\underset{\sim}{G}$ and f in Fig. 3, solve $\underset{\sim}{G}(0;\mu)\ f(\underset{\sim}{e};u) + \underset{\sim}{e} = 0$ for the equilibrium point $\hat{\underset{\sim}{e}}(\mu)$. Find the Jacobian matrix $\underset{\sim}{J}(\mu)$ of $\underset{\sim}{f}(\underset{\sim}{e};\mu)$ at $\hat{\underset{\sim}{e}}(\mu)$. Let $\hat{\lambda}(i\omega)$ be the eigenvalue of $\underset{\sim}{G}(i\omega)\underset{\sim}{J} \triangleq \underset{\sim}{G}(i\omega;\mu)\ \underset{\sim}{J}(\mu)$ whose intersection P_R with the real axis is nearest to the point $-1 + i0$. Let the resonant frequency associated with P_R be ω_R; i.e., identify ω_R such that $\text{Im}\ \hat{\lambda}(i\omega_R) = 0$. Find the normalized right eigenvector $\underset{\sim}{v}$ and the normalized left eigenvector $\underset{\sim}{u}$ of $\underset{\sim}{G}(i\omega_R)\underset{\sim}{J}$: $\underset{\sim}{G}(i\omega_R)\underset{\sim}{J}\ \underset{\sim}{v} = \hat{\lambda}(i\omega_R)\underset{\sim}{v}$ (a) $\underset{\sim}{u}^T\left[\underset{\sim}{G}(i\omega_R)\underset{\sim}{J}\right] = \hat{\lambda}(i\omega_R)\underset{\sim}{u}^T$ (b)
2	Form the ℓxm matrix $\underset{\sim}{Q}$ whose ikth element is: $Q_{jk} = \sum_{p=1}^{m} f_{pk}^{j}\, v_p,\ j = 1,2,\ldots,\ell;\ k = 1,2,\ldots,m$ (c) where $f_{pk}^{j} \triangleq \partial^2 f_j(\underset{\sim}{e})/\partial e_p \partial e_k$ (evaluated at $\hat{\underset{\sim}{e}}$).
3	Calculate $\underset{\sim}{v}^0 = -\frac{1}{4}\underset{\sim}{H}(0)\ \underset{\sim}{Q}\ \bar{\underset{\sim}{v}}$ (d) $\underset{\sim}{v}^2 = -\frac{1}{4}\underset{\sim}{H}(i2\omega_R)\underset{\sim}{Q}\ \underset{\sim}{v}$ (e) where $H(s) \triangleq \left[\underset{\sim}{G}(s)\underset{\sim}{J} + \underset{\sim}{1}\right]^{-1} \underset{\sim}{G}(s)$
4	Use (a), (c), (d), and (e) to calculate $\underset{\sim}{p}(\omega_R,\underset{\sim}{v}) = \underset{\sim}{Q}\ \underset{\sim}{v}^0 + \frac{1}{2}\bar{\underset{\sim}{Q}}\ \underset{\sim}{v}^2 + \frac{1}{8}\underset{\sim}{L}\ \bar{\underset{\sim}{v}}$ (f) where $\underset{\sim}{L}$ is an ℓxm matrix whose jkth element is: $L_{jk} = \sum_{p=1}^{m}\sum_{q=1}^{m} f_{pqk}^{j}\, v_p v_q,\ j = 1,2,\ldots,\ell;\ k = 1,2,\ldots,m$ (g) where $f_{pqk}^{j} \triangleq \partial^3 f_j(\underset{\sim}{y})/\partial y_p \partial y_q \partial y_k$ (evaluated at $\hat{\underset{\sim}{y}}$)
5	Use (a), (b), and (f) to calculate $\boxed{\zeta(\omega_R) = \dfrac{-\underset{\sim}{u}^T\underset{\sim}{G}(i\omega_R)\underset{\sim}{p}(\omega_R,\underset{\sim}{v})}{\underset{\sim}{u}^T\underset{\sim}{v}}}$ (h)

LIST OF FIGURE CAPTIONS

Fig. 1. Two phase portraits which are identical in a small neighborhood of the equilibrium point, but which differ significantly farther out: the limit cycle in (a) occurs when $\mu > \mu_o$ (super-critical case) and is locally stable. The limit cycle in (b) occurs when $\mu \leq \mu_o$ (sub-critical case) and is unstable.

Fig. 2. Loci of limit cycles as a function of the parameter μ. Each cross section of the bowl corresponds to a limit cycle. Solid bold lines denote minimal attractors while dotted lines denote minimal repellers. Bifurcation occurs at $\mu = \mu_o$. The limit cycles in (a) occur when $\mu \geq \mu_o$ (super-critical case) and is locally stable because the bowl is the right way up. The limit cycles in (b) occur when $\mu \leq \mu_o$ (sub-critical case) and is unstable because the bowl is upside down. The local nature of the equilibrium point ($x_1=x_2=0$) is identical for all values of μ in both cases. However, at $\mu = \mu_o$, the center is a vague attractor in (a) and a vague repeller in (b).

Fig. 3. A nonlinear multiple feedback loop representation, (a), and its linearized feedback system (b). The transfer matrix G is an $m\times\ell$ matrix. The $\ell\times m$ matrix $\underset{\sim}{J}$ in (b) denotes the Jacobian matrix of the nonlinear map $\underset{\sim}{f}: \mathbb{R}^m \to \mathbb{R}^\ell$ in (a).

Fig. 4. Graphical interpretation of the frequency-domain Hopf bifurcation theorem. The vector from the point -1 + i0 in the direction $\zeta(\hat{\omega})$ is shown calibrated in units of $\hat{\theta}^2|\zeta(\omega_R)|$; namely, the distance between the points -1 + i0 and $\hat{P}(\omega=\hat{\omega})$.

Fig. 5. An illustration of the application of the time and frequency-domain Hopf bifurcation theorem for analyzing an almost sinusoidal tunnel diode oscillator (Example 1). A locally stable limit cycle appears for all $\mu_o \leq \mu \leq \mu_o'$.

Fig. 6. An illustration of the application of the frequency-domain Hopf bifurcation theorem for analyzing the almost sinusoidal Wien bridge oscillator (Example 2). Observe that neither $\underset{\sim}{G}(s)$ nor $\underset{\sim}{J}(\mu)$ is a square matrix in this example.

Fig. 7. An illustration of the application of the frequency-domain Hopf bifurcation theorem for analyzing a biological oscillator (Example 3). Even though the dimension "n" of the state space can be quite large, the nonlinear map $\underset{\sim}{f}$ is only 2-dimensional.

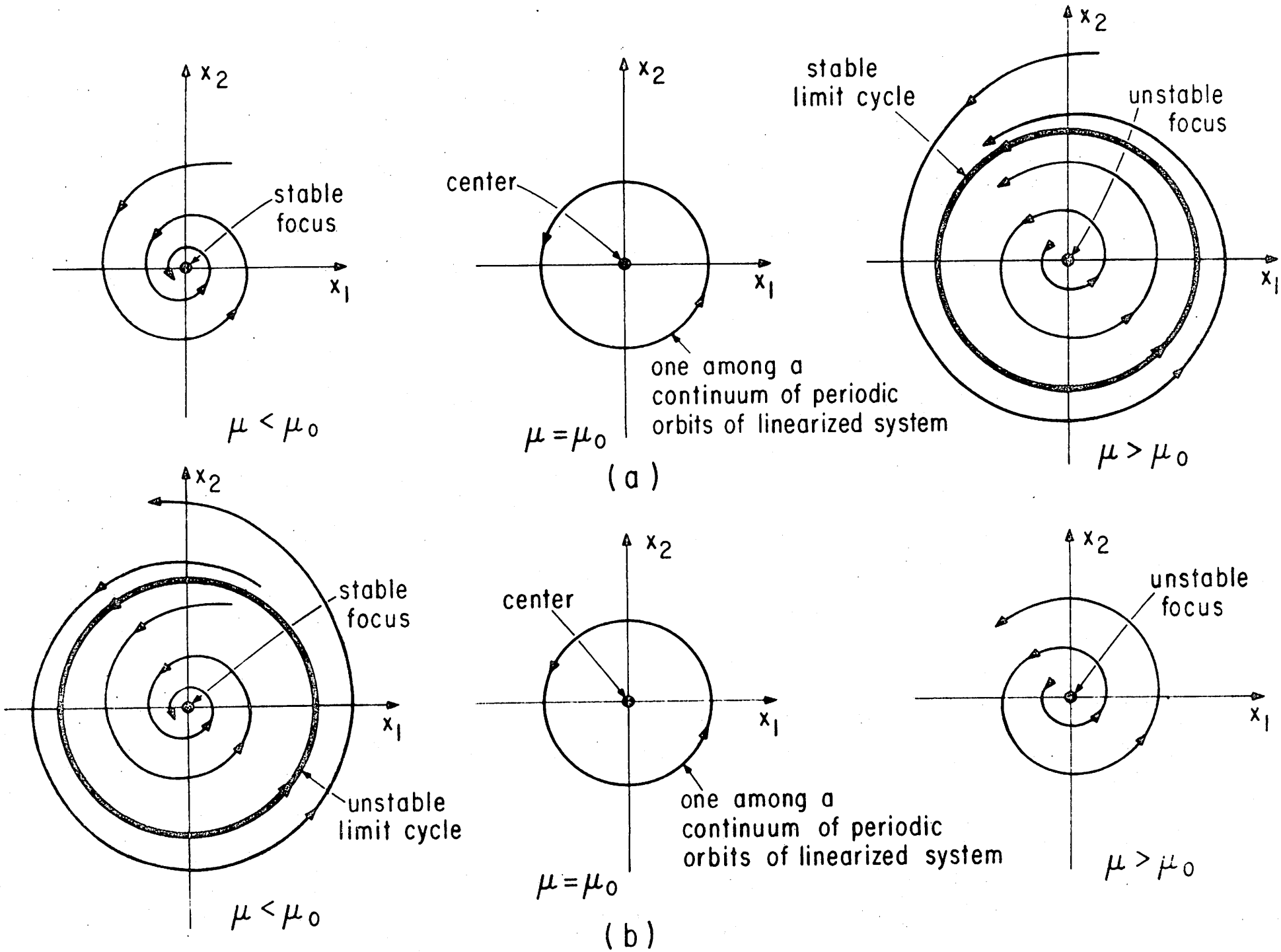
x2
x1
stable
focus
μ < μ0
center
one among a
continuum of periodic
orbits of linearized system
μ = μ0
stable
limit cycle
unstable
focus
μ > μ0
(a)
stable
focus
unstable
limit cycle
μ < μ0
center
one among a
continuum of periodic
orbits of linearized system
μ = μ0
unstable
focus
μ > μ0
(b)

Fig. 1

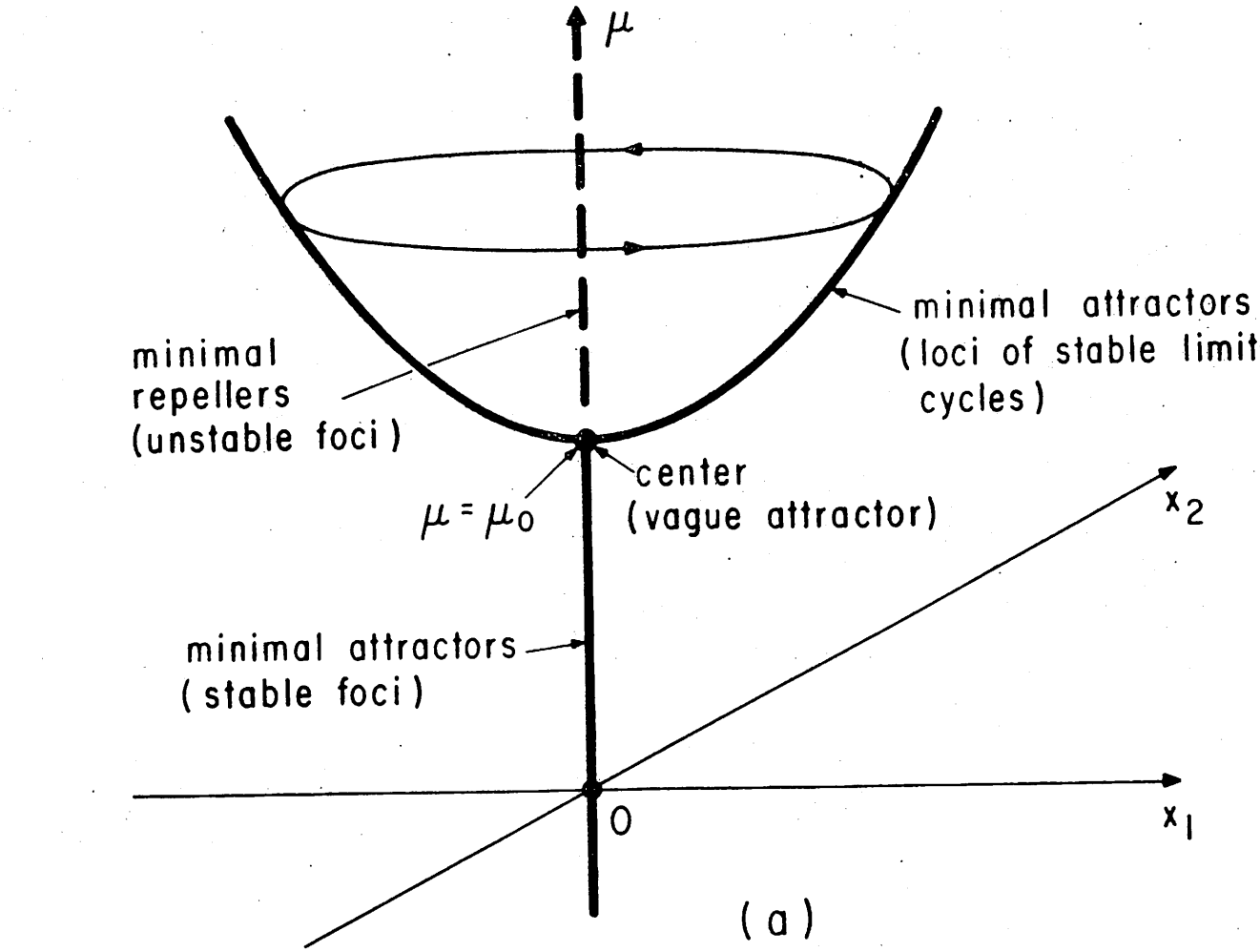
μ
minimal attractors
(loci of stable limit
cycles)
minimal
repellers
(unstable foci)
center
(vague attractor)
μ = μ0
x2
minimal attractors
(stable foci)
0
x1
(a)

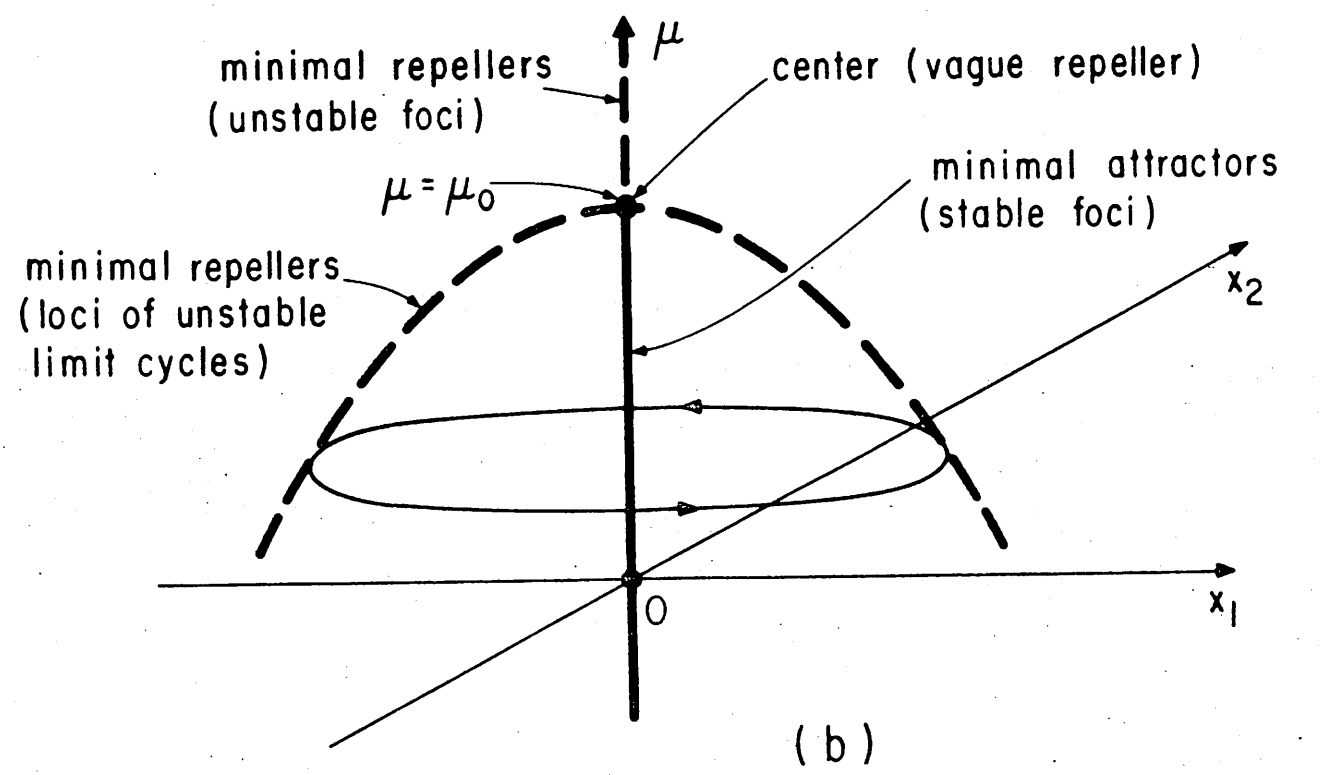
μ
minimal repellers
(unstable foci)
center (vague repeller)
μ = μ0
minimal attractors
(stable foci)
minimal repellers
(loci of unstable
limit cycles)
x2
0
x1
(b)

Fig. 2

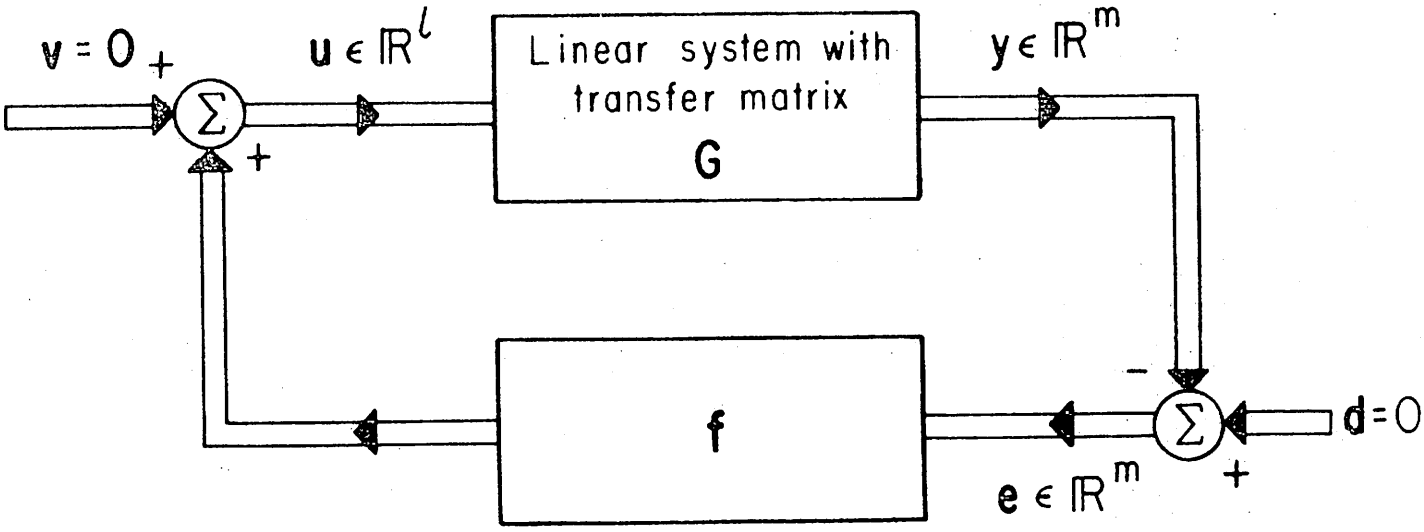
v = 0
+
u ∈ R^l
Linear system with transfer matrix G
y ∈ R^m
+
f
-
d = 0
e ∈ R^m
+

(a)

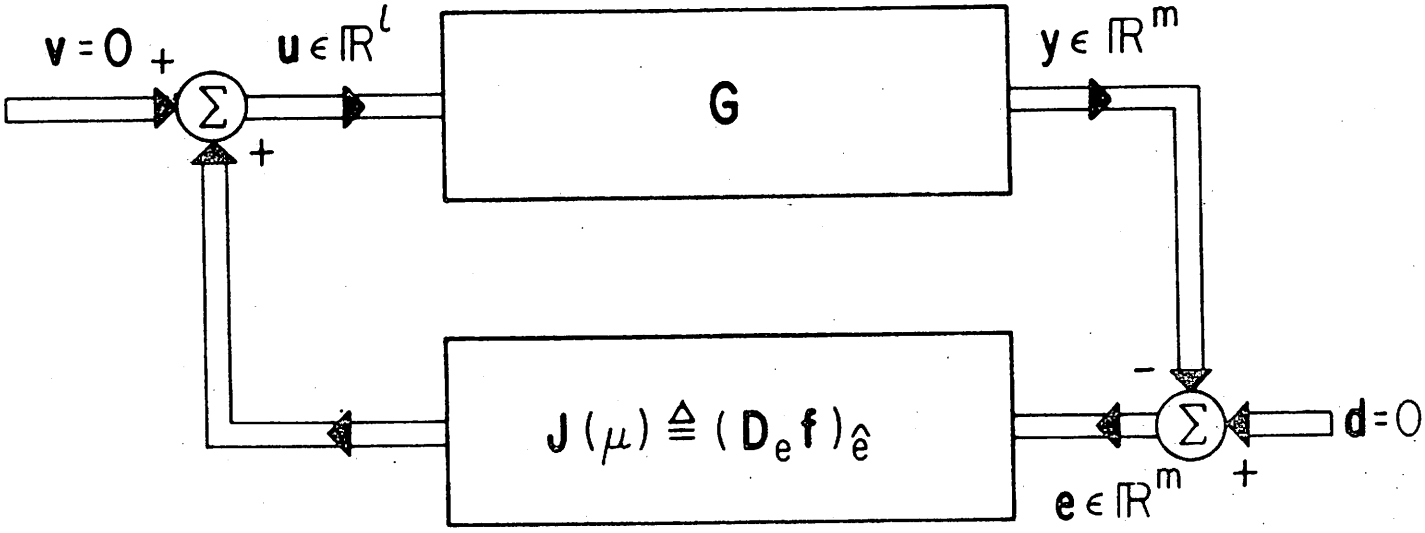
v = 0
+
u ∈ R^l
G
y ∈ R^m
+
J(μ) ≜ (D_e f)_ê
-
d = 0
e ∈ R^m
+

(b)

Fig. 3

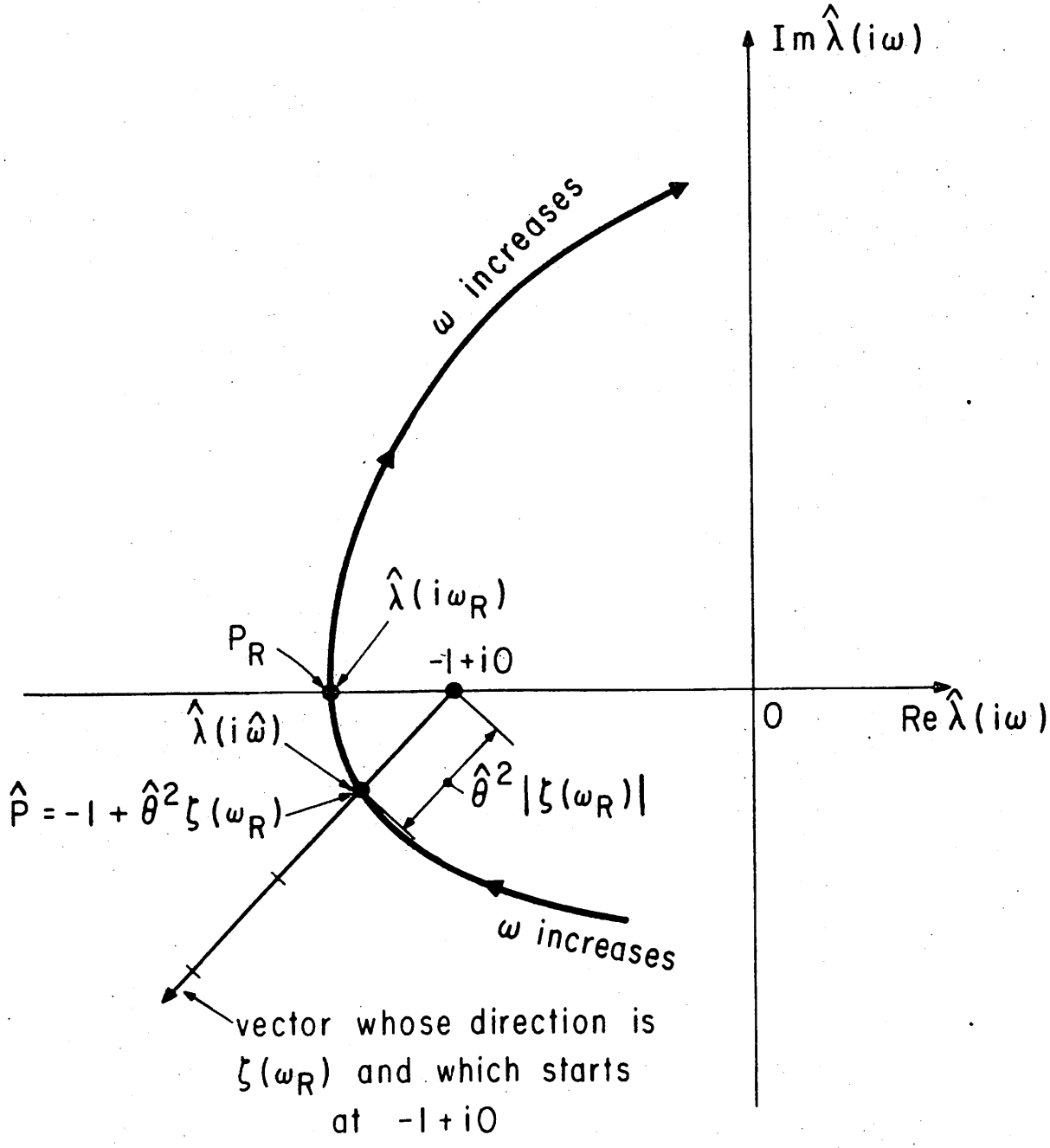
Im $\hat{\lambda}(i\omega)$
ω increases
$\hat{\lambda}(i\omega_R)$
P_R
$-1+i0$
$\hat{\lambda}(i\hat{\omega})$
0
Re $\hat{\lambda}(i\omega)$
$\hat{P} = -1 + \hat{\theta}^2\zeta(\omega_R)$
$\hat{\theta}^2|\zeta(\omega_R)|$
ω increases
vector whose direction is
$\zeta(\omega_R)$ and which starts
at $-1+i0$

Fig. 4

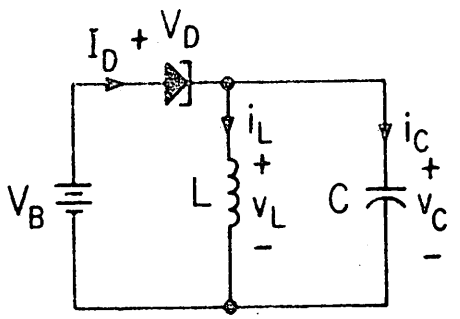

(a)

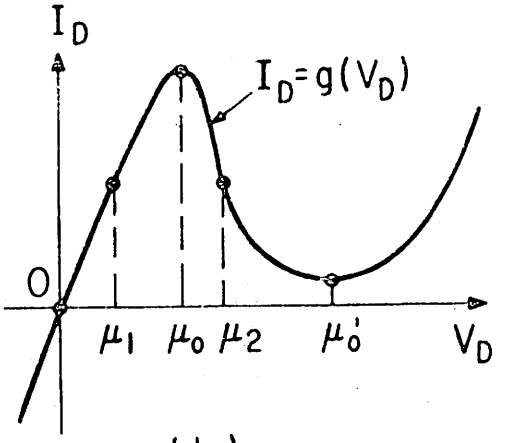

(b)

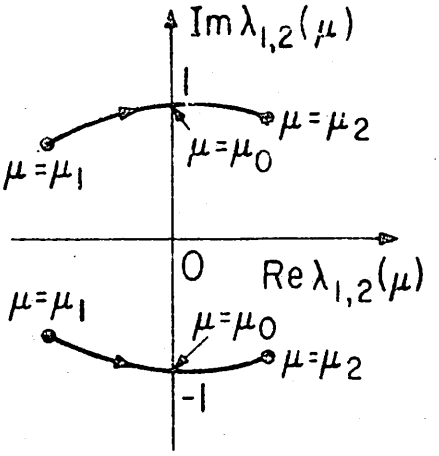

(c)

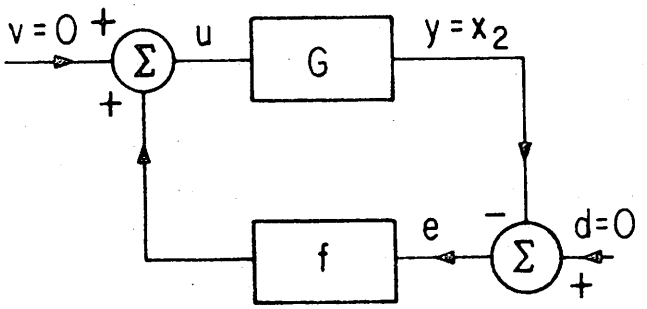

$$G(s) = \frac{s}{s^2+s+1}$$

$$f(e) = -g(\mu - e) - e$$

(d)

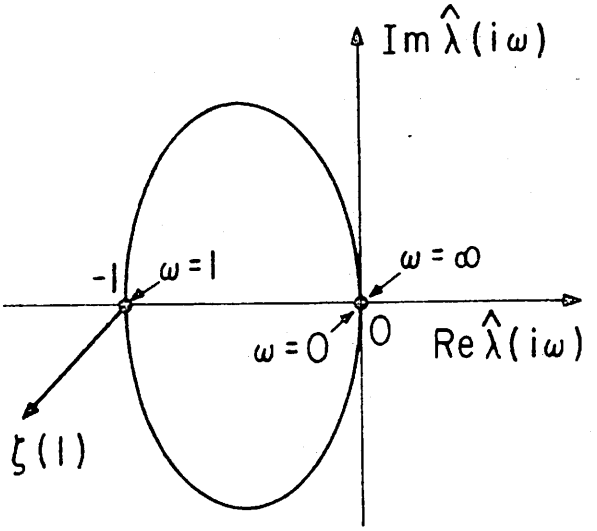

$$\hat{\lambda}(i\omega) = \frac{-\omega^2 - i\omega(1-\omega^2)}{(1-\omega^2)^2 + \omega^2}$$

(e)

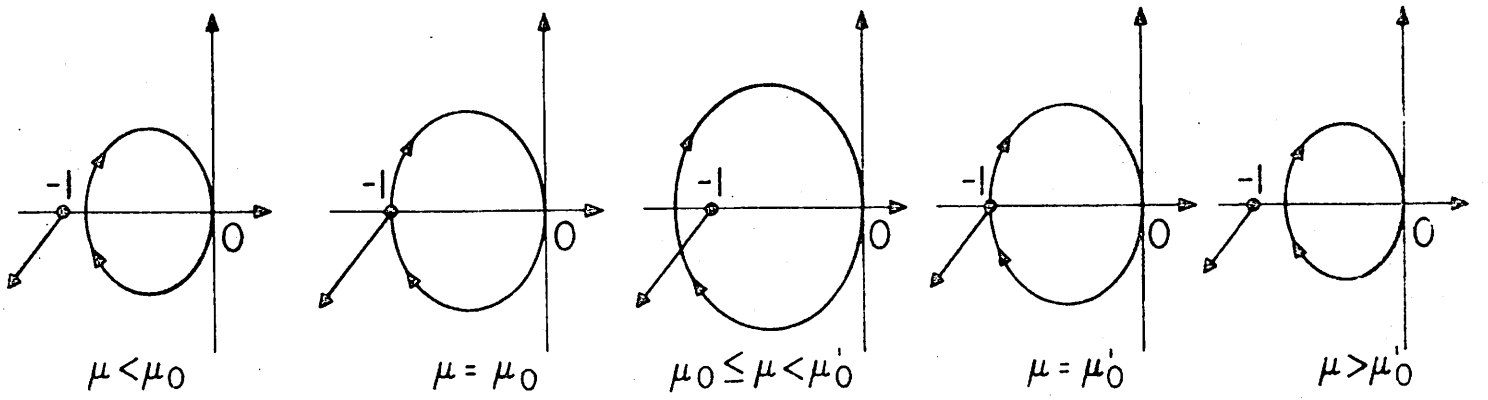

(f) (g) (h) (i) (j)

Fig. 5

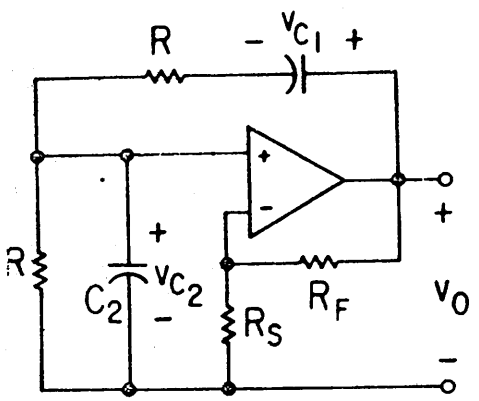

(a)

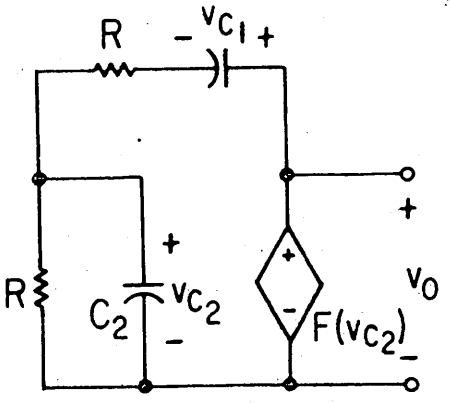

(b)

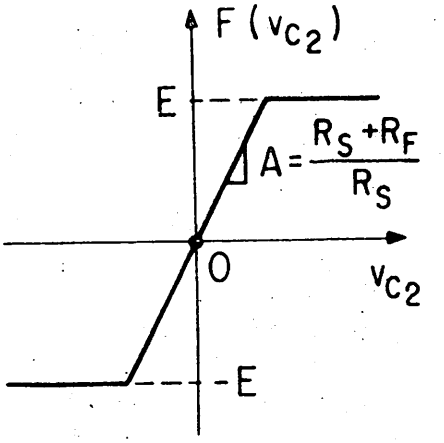

(c)

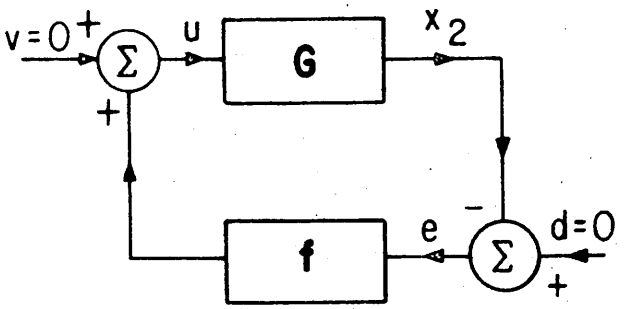

$$\mathbf{G}(s) = \begin{bmatrix} \frac{1}{s^2+3s+1} & \frac{-(s+1)}{s^2+3s+1} \end{bmatrix}$$

$$\mathbf{f}(e) = \begin{bmatrix} F(e) \\ F(e) \end{bmatrix}$$

(d)

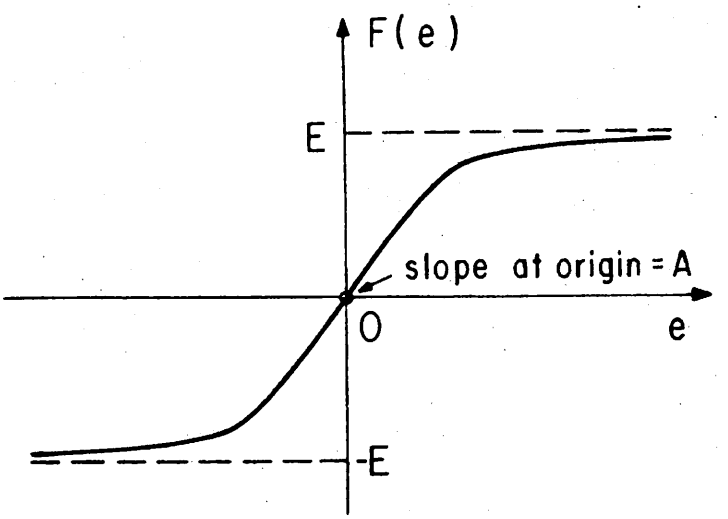

(e)

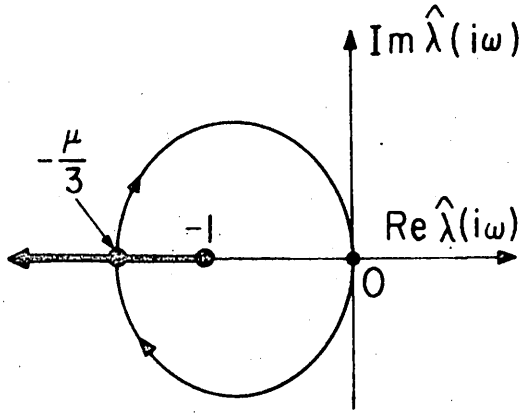

$\mu > 3$

(f)

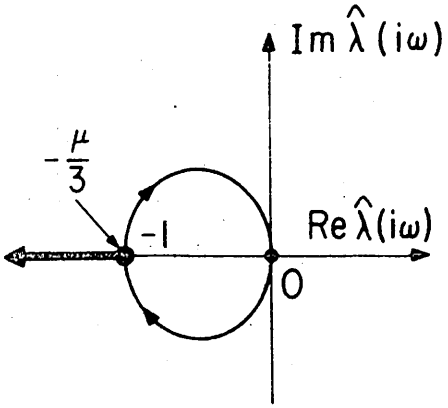

$\mu = 3$

(g)

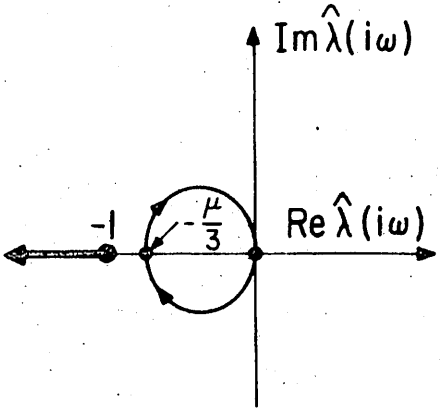

$\mu < 3$

(h)

Fig. 6

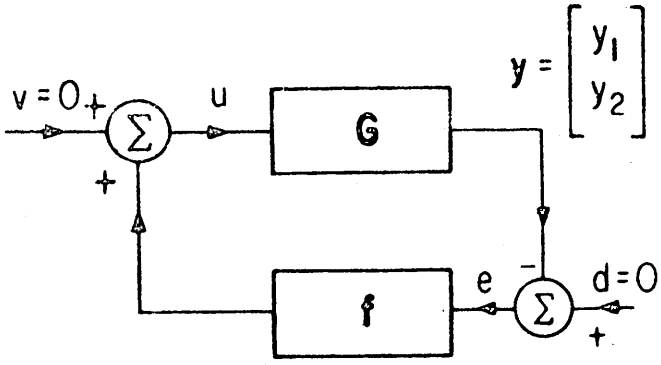

$$G(s) = \begin{bmatrix} \dfrac{1}{(s+b_1)} & 0 \\ 0 & \dfrac{1}{(s+b_2)(s+b_3)\cdots(s+b_n)} \end{bmatrix}$$

$$f(e) = \begin{bmatrix} \dfrac{-1}{1+e_2} \\ \dfrac{-e_1}{1+e_2} \end{bmatrix}$$

(a)

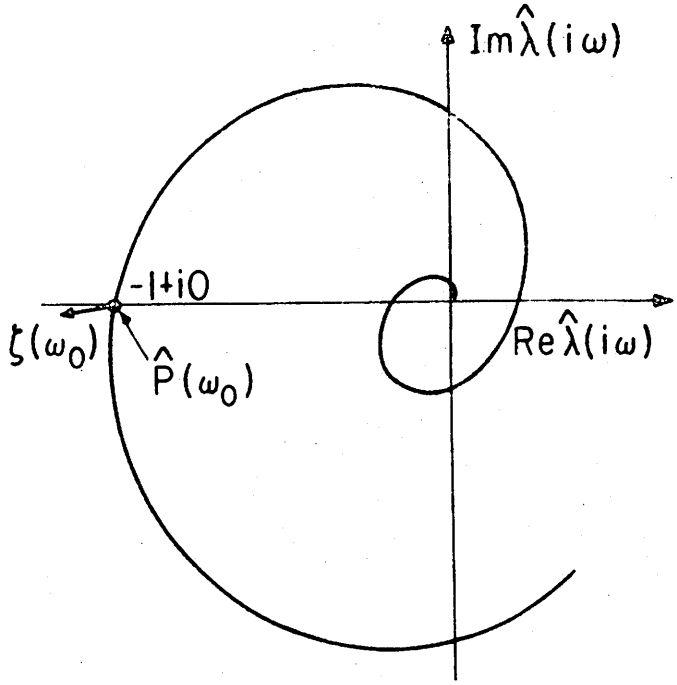

$b_j = 0.799$, $j = 1, 2, \ldots, n$

(b)

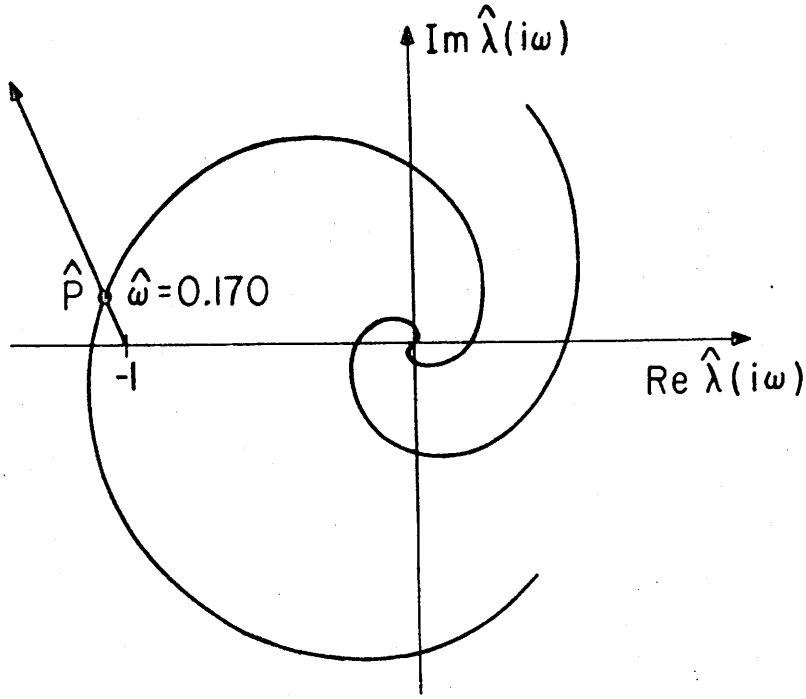

$b_j = 0.70$, $j = 1, 2, \ldots, n$

(c)

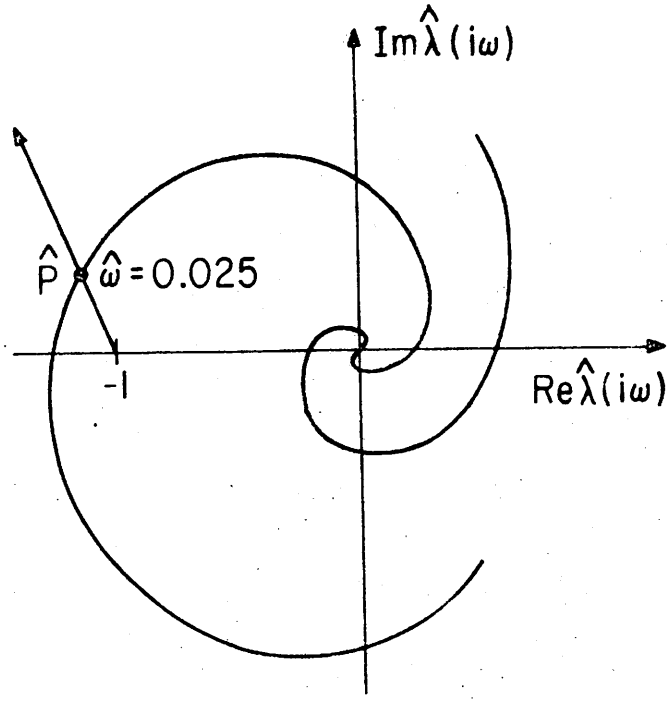

$b_j = 0.10$, $j = 1, 2, \ldots, n$

(d)

Fig. 7